DOI:10.1111/j.1600-0625.2010.01084.x
www.blackwellpublishing.com/EXD

Original Article

Ultraviolet light induces Stat3 activation in human keratinocytes and fibroblasts through reactive oxygen species and DNA damage

Toshinori Bito[1,2], Naoko Sumita[1], Taro Masaki[1], Toshiro Shirakawa[3], Masato Ueda[1], Ryutaro Yoshiki[2], Yoshiki Tokura[2] and Chikako Nishigori[1]

[1]Division of Dermatology, Department of Clinical Molecular Medicine, Kobe University Graduate School of Medicine, Kobe, Japan;
[2]Department of Dermatology, University of Occupational and Environmental Health, Kitakyushu, Japan;
[3]International Center for Medical Research and Treatment, Kobe University Graduate School of Medicine, Kobe, Japan
Correspondence: Dr Toshinori Bito, Department of Dermatology, University of Occupational and Environmental Health, 1-1 Iseigaoka, Yahatanishi-ku, Kitakyushu, 807-8555, Japan, Tel.: 81 93 691 7445, Fax: 81 93 691 0907, e-mail: bito@med.kobe-u.ac.jp

Accepted for publication 27 January 2010

Abstract: Stat3 is activated by the outer stressors, such as ultraviolet (UV) exposure. In this study, we investigated the Stat3 response to UV irradiation in human epidermal keratinocytes and dermal fibroblasts. Results indicated that UVB and UVC differentially activate Stat3 in these cells. The UV-induced Stat3 activation was mediated by both reactive oxygen species (ROS) and DNA damage, and the dominancy of ROS and DNA damage to activate Stat3 depended on the wavelength of UV. By using fibroblasts from a patient with xeroderma pigmentosum A (XP-A) and those transfected with human *XPA* gene, we found that UVB activates Stat3 *via* both ROS and DNA damage, while UVC does so mainly *via* DNA damage. The present data suggest that Stat3 activation in UV-exposed human skin is one of the initial events where DNA damage and ROS are involved.

Key words: DNA – reactive oxygen species – skin – Stat3 – UV

Please cite this paper as: Ultraviolet light induces Stat3 activation in human keratinocytes and fibroblasts through reactive oxygen species and DNA damage. Experimental Dermatology 2010; **19**: 654–660.

Introduction

In aged individuals, accumulative exposure to ultraviolet (UV) light from the sun, particularly its UVB component (290–320 nm), to the skin is a major cause for the development of skin cancers. Photoageing is caused by cumulative sun exposure in addition to chronologic ageing. To avoid photoageing including skin cancer development, the molecular mechanisms underlying UV-induced skin damage need to be elucidated. Fisher et al. have revealed that the UV irradiation activates signalling pathways such as ERK 1/2 which upregulates expression and functional activation of a nuclear transcription factor, AP-1, resulting in diverse response including photoageing (1). UV also activates NF-κB that stimulates the transcription of proinflammatory cytokine genes, which reversely acts through their surface receptors to further stimulate AP-1 and NF-κB, thereby amplifying the UV response (1). Thus, UV is suggested to be an important cue to evoke a series of biological responses *in vivo*.

Abbreviations: STAT, signal transducer and activator of transcription; UV, ultraviolet; XP, xeroderma pigmentosum.

On the other hand, a recent study has reported that UVB activates another transcription factor, signal transducer and activator of transcription 3 (Stat3) in the skin of hairless mouse (2). Stat3 has been expected as a target for the management of skin cancer. Signal transducers and activators of transcription (STATs) are activated in response to a variety of cytokines and growth factors. The STAT family has seven known members in mammals, Stat1, Stat2, Stat3, Stat4, Stat5a, Stat5b and Stat6. Among the STATs, Stat3 has been implicated to have a potential to prevent apoptotic signalling in cells (3). Sano et al. have reported that Stat3 activation rescues the UVB-induced apoptosis of keratinocytes in hairless mouse (4). As the previous studies revealed the constitutive activation of Stat3 in various human cancers (5–7), Stat3 is recognized as an oncogene (8). These various observations have led to the current concept that Stat3 plays a more important role than does AP-1 or NF-κB for photocarcinogenesis. However, the roles of Stat3 in the human skin and relating disorders remain unclear. Previously, we have reported that the inhibition of Stat3 activity is not sufficient to induce apoptosis, although Stat3 activation is required for cell proliferation and tumorigenesis for cutaneous squamous cell

Experimental Dermatology

carcinoma (9). Accumulated evidence supports that Stat3 activation prevents the cell death from various damage including UV. Human cells are protected from a variety of external stressor by activating Stat3, resulting in enhancement of survival. Nevertheless, excess activation of Stat3 may also yield unexpected outcomes such as cancer.

In this study, we investigated the initial signalling pathway following UV irradiation in human epidermal keratinocytes and dermal fibroblasts, focusing on Stat3. To further address the mechanism underlying the UVB-induced Stat3 activation, human fibroblasts from a patient with xeroderma pigmentosum A (XP-A) having repair deficiency in UV-induced DNA damage were also subjected. Results indicate that Stat3 is activated by UVB in human keratinocytes and fibroblasts in a different manner.

Materials and methods

Cells, cell culture and treatment

Primary normal human epidermal keratinocytes (HEK) and normal fibroblasts were purchased from KURABO (Osaka, Japan). HEK were grown in keratinocyte serum–free medium supplemented with human keratinocyte growth supplement and penicillin, streptomycin and amphotericin B (PSA) solution (Gibco, Grand Island, NY, USA). Primary human fibroblasts were obtained from a patient with XP-A, after obtaining a written informed consent, and was designated XP1MG (10). They were grown in Dulbecco's modified Eagle's minimum essential medium (Invitrogen Co., Carlsbad, CA, USA) supplemented with 15% foetal bovine serum (HyClone, Logan, UT, USA) and maintained in a humidified air containing 5% CO_2 at 37°C. The regular medium for the both cells was replaced with the medium without growth supplement, PSA or serum 24 h before UV irradiation. Buthionine sulfoximine (BSO) and (±) α-lipoic acid (LA) were purchased from Sigma Chemicals Co. (St Louis, MO, USA). BSO was freshly dissolved in DMSO at 100 mM. LA was prepared in distilled water at 50 mM, and adjusted with 1 M NaOH to pH8.0. HEK were pretreated with 100 μM of BSO or 500 μM of LA for 24 h before UV exposure. After nine of 10-ml medium was removed, cells were irradiated with UV and replaced with the medium containing LA immediately after the exposure. UV-absorbance of LA of our working condition was recorded from 260 to 390 nm using a Beckman DU-70 spectrophotometer.

UV irradiation

FL20SE fluorescent lumps (Toshiba Electric Co., Tokyo, Japan) were used as a source of UVB. These lamps emit mainly wavelengths between 280 and 360 nm, peaking at 311 nm. Flux intensity was measured with an UVR-305/365D UV radiometer (Tokyo Optical Co Ltd, Tokyo, Japan). Germicidal lamps predominantly emitting 254 nm (GL10; Toshiba Electric Co.) were used as a source of UVC. Fluence rates were measured by the UV radiometers, UV-254 (Topcon; Tokyo Kogaku Kikai KK, Tokyo, Japan).

Electrophoretic mobility shift assay

Nuclear extracts from the cells were prepared following the method described by Corsini et al. (11), with slight modifications. Electrophoretic mobility shift assay (EMSA) was performed essentially as described earlier (12). Binding reaction mixtures (20 μl) containing 5 μg nuclear extract protein, 2 μg poly (dI-dC) (Amersham Pharmacia Biotech, Piscataway, NJ, USA), ^{32}P-labelled probe (Stat3), 50 mM NaCl, 2 mM $MgCl_2$, 0.2 mM Na_2EDTA, 1 mM DTT, 10% (v/v) glycerol and 4 mM Tris–HCl (pH 7.9) were incubated for 30 min at room temperature. Proteins were separated by electrophoresis in native 6% polyacrylamide gels using a Tris-borate-EDTA running buffer (12.5 mM Tris-borate containing 0.25 mM Na_2EDTA, pH 8.0), followed by autoradiography. The Stat3 probe (Santa Cruz Biotechnology, Santa Cruz, CA, USA) was labelled with [γ-^{32}P] dATP (Du Pont NEN, Boston, MA, USA) using T4 polynucleotide kinase (Boehringer MannheimRoche, Mannheim, Germany).

Immunoblot analysis

Cells were washed with ice-cold D-PBS containing 200 μM sodium orthovanadate (Na_3VO_4), frozen immediately in liquid nitrogen, and then lysed in lysis buffer (25 mM Tris–HCl, pH 7.6, 200 mM boric acid, 150 mM NaCl, 50 mM NaF, 5 mM Na_2EDTA, 1% Triton X-100, 10 mM sodium pyrophosphate, 2 mM EGTA, 20 mM p-nitrophenyl phosphate, 1% BSA, 20 μM Na_3VO_4 and 2 mM DTT) containing protease inhibitors (2 μg/ml each of aprotinin, leupeptin, pepstain, antipain and 100 μg/ml PMSF). The lysates were centrifuged at 10 000 × *g* at 4°C for 15 min, and the resulting supernatants were subjected to immunoblot analysis. Protein concentrations in the supernatants were quantitated by the Coomassie® plus protein assay reagent (Bio-Rad). Samples (20 μg protein each) for immunoblotting were separated on 8% polyacrylamide gels for Stat3 by SDS–polyacrylamide gel electrophoresis and were blotted onto Hybond-ECL nitrocellulose membranes (Amersham Pharmacia Biotech). The membranes were blocked with 5% skim milk in Tris-buffered saline for 2 h at room temperature and were then probed with primary polyclonal antibodies to phospho-Stat3 (p-Tyr705 or p-Ser727) antibody (Cell Signalling Technology, Beverly, MA, USA) overnight at 4°C, and then incubated with corresponding horseradish peroxidase-conjugated secondary antibodies at room temperature for 1 h. Bound antibody was detected with Immunostar Reagents (Wako, Osaka, Japan). The membranes were exposed to Hyperfilm (Amersham Pharmacia Biotech). After the film exposure, the

membranes were washed four times for 5 min each in PBS-Tween 20, and were then incubated for 30 min at 50°C in stripping buffer (62.5 mM Tris–HCl pH 6.8, 2% SDS and 100 mM 2-mercaptoethanol). The membranes were blocked with 5% skim milk again, and then reprobed with an antibody to total Stat3 protein (Cell Signalling Technology), or reblotted with human actin (Santa Cruz Biotechnology) as a loading control overnight at 4°C, and then incubated with corresponding horseradish peroxidase-conjugated secondary antibodies. Quantification of protein expression was performed using NIH image analysis software (version 1.62f) (Bethesda, MD, USA).

Immunofluorescence

Human epidermal keratinocytes were plated on Lab-Tek® chamber slides (Nalge Nunc International, Naperville, IL, USA). Two-day-cultured cells were left untreated or treated with LA for 24 h and exposed to UVB. After UV exposure, the cells were incubated for 15 min and fixed with 3% formaldehyde in PBS for 15 min at room temperature followed by permeabilization with ice-cold methanol for 10 min. The slides were rinsed in PBS and incubated for 18 h at 4°C with phospho-Stat3 (p-Tyr705 or p-Ser727) antibody (Cell Signalling Technology) diluted in 0.3% Triton X-100 in PBS following blocking in 5% normal rabbit serum for 60 min. After incubation, the slides were washed three times in PBS and incubated with fluorochrome-conjugated secondary anti-rabbit antibody for 1 h. Following two washes in PBS, the slides were mounted with Prolong® Gold Antifade Reagent (Invitrogen Co.). Fluorescence was examined by a laser scanning confocal imaging microscope and processed with LSM Image Browser (Carl Zeiss, Tokyo, Japan).

Electroporation

Plasmids containing human *XPA* gene, pcHA-*XPA*, constructed from pcDNA3 inserting *XPA* cDNA and Influenza haemaggultinin gene (HA) as a tag (kindly provided by Dr Kiyoji Tanaka), was transfected into XP1MG by an electroporation method (350 kV, 1.5 ms) using the ECM 830 electroporation system (BTX, San Diego, CA, USA). XPA protein and HA after electroporation were detected by Western blotting using monoclonal antibody against human XPA and HA. XP1MG cells transfected with pcHA-*XPA* were harvested and inoculated into 6-well cell culture plates at the density of 2×10^5 cells/well for 12 h, and then exposed to UVC. The cell lysates were utilized for immunoblotting.

Statistical analyses

Data are expressed as means ± standard deviations. Statistical analyses were performed using Prism 5 software (GraphPad Software, San Diego, CA, USA). Unpaired experimental groups were compared with the Student's *t*-test. $P < 0.05$ was considered significant.

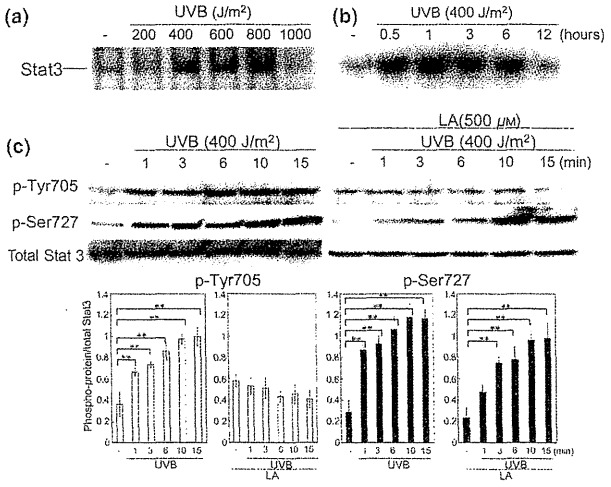

Figure 1. UVB-induced DNA binding activity and phosphorylation of Stat3 in human epidermal keratinocytes (HEK). Nuclear extracts from the cells under the regular condition were analysed using EMSA with a ^{32}P-labelled DNA probe to detect DNA binding activity of Stat3. (a) HEK were collected 30 min after UVB irradiation, and nuclear extracts were subjected to EMSA. (b) A kinetics analysis was performed after 400 J/m^2 of UVB irradiation. Data are a representative of three independent experiments. (c) HEK were exposed to 400 J/m^2 of UVB without or with 500 μM of LA pretreatment for 24 h and collected at the indicated time points. The cell lysates (20 μg) were immunoblotted with each of the anti-p-Stat3 (p-Tyr705) antibody, or p-Stat3 (p-Ser727) antibody and reprobed with an anti-Stat3 (total) antibody as a loading control. Data are a representative of three independent experiments. The bar graphs are expressed as the relative ratio of phospho-Stat3 protein expression to total Stat3 protein expression by densitometry using NIH image analysis software. Data are mean ± SD of three independent experiments. $^{**}P < 0.01$ are statistically significant when compared with the non-treated control.

Results

UVB-induced Stat3 activation in HEK

Stat3 DNA binding activity was examined following single UVB exposure in HEK. HEK were exposed to UVB and collected 30 min later. Nuclear extracts from the cells were analysed by EMSA. Stat3 was activated in a dose-dependent manner from 400 to 800 J/m^2 of UVB irradiation (Fig. 1a). A kinetics analysis was performed following 400 J/m^2 of UVB irradiation. Stat3 was activated 30 min after UVB irradiation, and its activation continued for 6 h and returned to the baseline 12 h after UVB exposure (Fig. 1b).

UVB upregulated Stat3 phosphorylation at both Tyr705 and Ser727 and antioxidants suppressed UVB-induced Stat3 activation markedly at Tyr705 and partially at Ser727

Stat3 activation requires the phosphorylation at both tyrosine 705 (Tyr705) and serine 727 (Ser727) in stimulation with cytokines or growth factors. Therefore, we investigated

the phosphorylation of Tyr705 and Ser727 of Stat3 in UVB-exposed HEK by immunoblot analysis. HEK were irradiated with 400 J/m^2 of UVB and harvested at 1, 3, 6, 10 and 15 min after UVB irradiation. The cell lysates (20 μg) were immunoblotted with an anti-p-Stat3 (p-Tyr705), or p-Stat3 (p-Ser727) antibody and reprobed with an anti-Stat3 (total) antibody as a loading control. Both p-Tyr705 and p-Ser727 protein levels were upregulated at 1 min after UVB irradiation, and that upregulation continued at least for 15 min (Fig. 1c, left panel).

UVB is well known to generate reactive oxygen species (ROS), whereas UVC generates little amount of ROS (13). The cellular level of glutathione (GSH), which carries scavenge system for ROS in cells, can be elevated by lipoic acid (LA), a precursor of GSH. To verify the influence of ROS, HEK were pretreated with antioxidants, LA (500 μM) for 24 h and exposed to UVB under the same condition as was performed without LA. LA treatment suppressed the UVB-induced upregulation of p-Tyr705 at all the time points examined, but LA treatment suppressed the UVB-induced p-Ser727 only slightly (Fig. 1c, right panel). The absorbance of LA at this range was almost negligible at our experimental condition. In addition, flux intensity was measured using UV radiometer through the medium with or without LA at the concentration. Each medium showed the same intensity as 0.98 mW/cm^2. An immunofluorescence analysis further supported the differential phosphorylation of Tyr705 and Ser727 in keratinocytes (Fig. 2). The protein expression of p-Tyr705 was seen both in the nuclei and in the cytoplasm 15 min after 400 J/m^2 of UVB, and again the protein

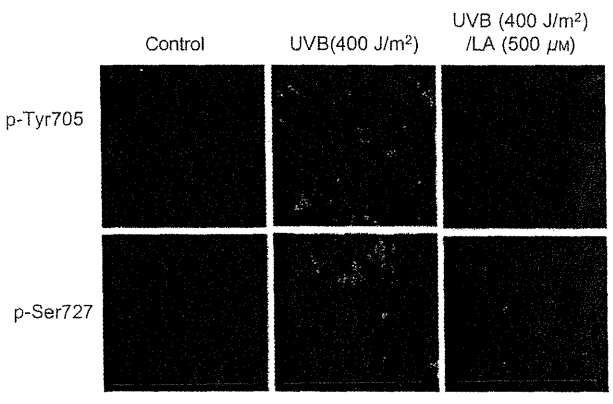

Figure 2. Localization of phosphorylated forms of Tyr705 and Ser727 following UVB irradiation. human epidermal keratinocytes were plated on the chamber slides. The cells after 2 days of culture were left untreated or treated with LA for 24 h and then exposed to 400 J/m^2 of UVB. The protein expression of p-Tyr705 or p-Ser727 was examined using a laser scanning confocal imaging microscope in fluorescence 15 min after UVB irradiation. The protein expression of p-Tyr705 was seen in both the nuclei and the cytoplasm, and the protein expression was suppressed with 500 μM of LA pretreatment. The protein expression of p-Ser727 was seen predominantly in the nulcei, and LA pretreatment exerted a weak suppression.

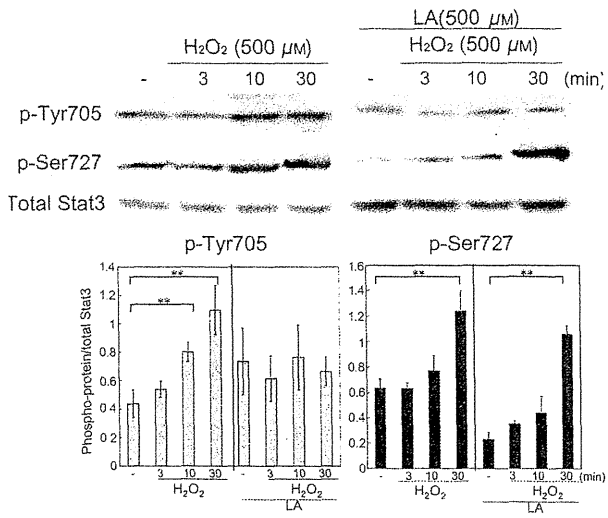

Figure 3. Hydrogen peroxide-induced Stat3 phosphorylation at both Tyr705 and Ser727 sites. human epidermal keratinocytes were incubated with 500 μM hydrogen peroxide (H_2O_2) without or with LA pretreatment for the indicated time. Data are a representative of three independent experiments. The bar graphs are expressed as the relative ratio of phospho-Stat3 protein expression to total Stat3 protein expression by densitometry using NIH image analysis software. Data are mean ± SD of three independent experiments. $^{**}P < 0.01$ are statistically significant when compared with the non-treated control.

expression was suppressed by LA treatment. On the other hand, the expression of p-Ser727 was seen dominantly in the nulcei at the same time points after 400 J/m^2 of UVB, and LA treatment had little effect on the expression. Virtually no phospho-Stat3 protein was detected in HEK without stimuli. Next, to examine whether ROS activate Stat3 in HEK, HEK were incubated with hydrogen peroxide (H_2O_2) for the indicated period. Treatment with 500 μM of H_2O_2 for 10 and 30 min activated Stat3 on Tyr705, whereas Ser727 activation was observed only after 30 min treatment (Fig. 3). Pretreatment with LA abrogated the H_2O_2-induced upregulation of p-Tyr705 throughout the time course, but failed to abrogate the Ser727 phosphorylation (Fig. 3).

Phosphorylation of Stat3 by UVC at Ser727

UVB irradiation produces both DNA damage and membrane damage. To elucidate the mechanism of UVB-induced Stat3 activation, we employed UVC irradiation because UVC is known to preferentially cause DNA damage such as pyrimidine dimer and (6-4) CT photoproduct (13). Although our skin is not exposed to UVC irradiation, we used UVC as a procedure for DNA damage, while H_2O_2 served as a tool for membrane damage. HEK were irradiated with single exposure of UVC and were collected at 1, 3, 6, 10 and 15 min after UVC irradiation. P-Tyr705 was slightly upregulated at 6 and 10 min after UVC irradiation, but UVC totally caused little affect on p-Tyr705 protein (Fig. 4). On the other hand,

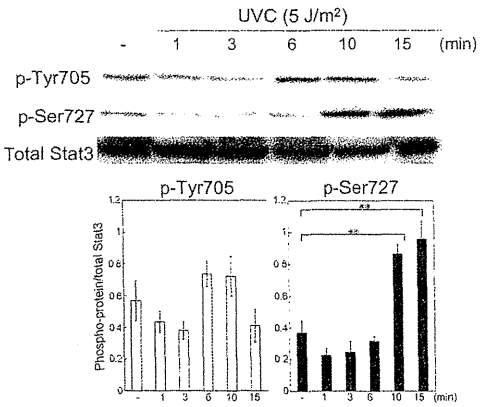

Figure 4. UVC-induced Stat3 phosphorylation at Ser727 site. human epidermal keratinocytes were irradiated with 5 J/m^2 of UVC and collected at the indicated time points. The cell lysates (20 μg) were immunoblotted with each of the anti-p-Stat3 (p-Tyr705) antibody, or p-Stat3 (p-Ser727) antibody and reprobed with an anti-Stat3 (total) antibody as a loading control. Data are a representative of three independent experiments. The bar graphs are expressed as the relative ratio of phospho-Stat3 protein expression to total Stat3 protein expression by densitometry using NIH image analysis software. Data are mean ± SD of three independent experiments. $^{**}P < 0.01$ are statistically significant when compared with the non-treated control.

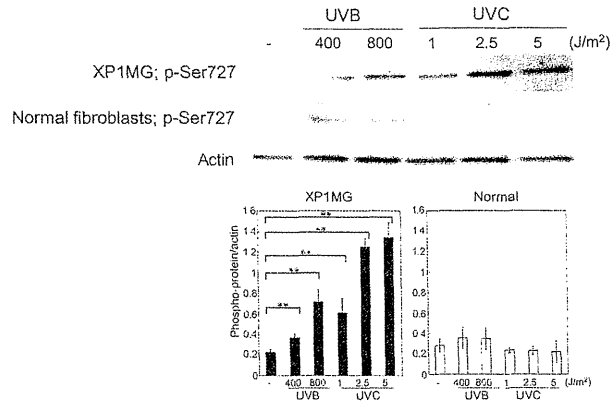

Figure 5. Phosphorylation of Stat3 by UVB or UVC irradiation in XP-A fibroblasts but not in normal fibroblasts. XP1MG fibroblasts or normal fibroblasts were irradiated by UVB (400 or 800 J/m^2) or UVC (1, 2.5 or 5 J/m^2) and collected 10 min after irradiation. The cell lysates (20 μg) were immunoblotted with anti-p-Stat3 (p-Ser727) antibody and reblotted with human actin as a loading control. Data are a representative of three independent experiments. The bar graphs are expressed as the relative ratio of phospho-Stat3 protein expression to actin protein expression by densitometry using NIH image analysis software. Data are mean ± SD of three independent experiments. $^{**}P < 0.01$ are statistically significant when compared with the non-treated control.

p-Ser727 was clearly elevated at 10 and 15 min. As UVB upregulated p-Ser727 protein earlier than UVC, each wavelength might exert phosphorylation in different mechanisms. BSO depletes cellular GSH and renders cells sensitive to ROS (14). The balance between the production rate of ROS and the function of GSH affects the intracellular reduction–oxidation status, which is crucial for the regulation of several cellular physiological functions. To assess the role of ROS in the UVC-induced Stat3 activation, the effect of LA and sublethal concentrations of BSO was examined. HEK were pretreated with LA (500 μM) or 100 μM of BSO and exposed to 5 J/m^2 of UVC. Phosphorylation levels neither at Tyr705 nor at Ser727 was affected by LA or BSO pretreatment (data not shown).

Upregulation of phospho-Stat3 at Ser727 by UVB and UVC in XP1MG fibroblasts

XP-A is an inheritated photosensitive disorder caused by repair deficiency in UV-induced DNA damage, and the responsible gene for XP-A is involved in DNA damage recognition in nucleotide excision repair (15). To ask whether pyrimidine dimer, major UV-induced DNA damage can be a trigger for Stat3 activation, Stat3 activity was examined using cells from a XP-A patient. Because keratinocytes from XP patients are neither commercially available nor available from the patient. We used the fibroblasts from the XP-A patient. Stat3 activation was compared between XP1MG, a fibroblast from a XP-A patient, and normal fibroblasts after UVB or UVC irradiation. No significant increase in Stat3 protein was observed in normal fibroblasts by 800 J/m^2 of UVB or 5 J/m^2 of UVC, whereas normal keratinocytes showed phosphorylation at Ser727 by the same doses of UVB and UVC (as shown in Figs 1c and 4). Fibroblasts look less responsive to UV damage in comparison with keratinocytes. However, single UVB or UVC irradiation dose-dependently induced Stat3 phosphorylation at Ser727 in XP1MG (Fig. 5). As for phosphorylation of Tyr705, no activation could be observed in XP1MG or normal fibroblasts by the same dose of UV, indicating that Ser727 was more sensitive to UV irradiation than Tyr705 in the fibroblasts (data not shown). To verify whether UV activates Ser727 of Stat3 through the DNA damages in XP1MG, pcHA-*XPA* was transfected into XP1MG. pcDNA3 was used as a control vector. Transfection of the *XPA* gene almost completely abrogated the UVC upregulation of Stat3 phosphorylated protein on Ser727, whereas the UVB-induced Stat3 phosphorylation was partially reduced (Fig. 6).

Discussion

We found that UVB activates Stat3 in human keratinocytes and fibroblasts in a manner different from each other. The UV-induced Stat3 phosphorylation is mediated by both ROS and DNA damage produced depending on the wavelength of UV. Accordingly, Grether-Beck et al. have shown that both UVA and UVB activate transcription factors such as AP1, AP2 or NF-κB in different manners (16).

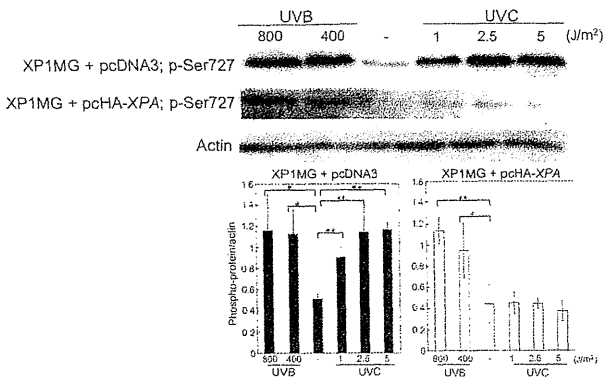

Figure 6. Transfection with *XPA* gene abrogated the UV-induced phosphorylation of Stat3 in XP1MG. XP1MG transfected with pcHA-*XPA* or control vector (pcDNA3) were irradiated with UVB (400 or 800 J/m^2) or UVC (1, 2.5 or 5 J/m^2) and were collected 10 min after irradiation. The cell lysates (20 μg) were immunoblotted with anti-p-Stat3 (p-Ser727) antibody and reblotted with human actin as a loading control. Data are a representative of three independent experiments. The bar graphs are expressed as the relative ratio of phospho-Stat3 protein expression to actin protein expression by densitometry using NIH image analysis software. Data are mean ± SD of three independent experiments. $*P < 0.05$ and $**P < 0.01$ are statistically significant when compared with the non-treated control.

Fisher et al. demonstrated that the activation of AP-1 and NF-κB mediates signalling pathways starting within 1 h after UV irradiation and reaches to the maximal within 4 h in human skin *in vivo* (1,17). On the other hand, Grether-Beck et al. have shown that both UVA and UVB induce an early activation observed immediately 30 min after UV treatment (16). The upregulation of Stat3 DNA binding activity was observed within 30 min after UVB irradiation in this study. In a specified condition, Simon et al. have shown that UVB is able to activate NF-κB in cytosolic extracts 20 min after treatment (18). Stat3 activation might precede AP-1 and NF-kB activation according to the situation, although it was difficult to compare it under the same condition. Our immunoblot analysis supported this notion, because Stat3 phosphorylation started within 1 min after UVB irradiation. Several previous reports using human or mouse skin *in vivo*, or *in vitro* have shown that the transcription factors are activated with UV or cytokine stimulation in a couple of hours (1,2,19,20). As far as we know, there have been no data showing such an immediate activation of transcription factors as Stat3 observed in this study. Stat3 is activated *via* the related kinases or cytokines such as epidermal growth factor receptor and IL-6 (21), and thus its activation seems to be mediated by the signalling pathways through cytokines or membrane receptors. Because of its rapid upregulation, however, UVB is suggested to activate Stat3 directly.

In this study, we found that DNA damage induces Stat3 phosphorylation. As UVC has a more potent ability to form DNA damage than UVB (22,23), we also used UVC to exclusively produce DNA damage. The similar effect of UVC to UVB on the upregulation of Stat3 protein was observed, although a slight delay of the response was seen by UVC. The pretreatment of LA diminished the UVB-induced Stat3 activation. Morphological observations by immunohistochemical method revealed that the protein expression of p-Tyr705 and p-Ser727 Stat3 was present in the cytoplasm and nuclei in the keratinocytes. The potent suppressive effect of an antioxidant, LA, on phosphorylation at Tyr 705 was clearly shown in the experiment using H_2O_2 as a stimulus, strongly suggesting the involvement of ROS in the phosphorylation at this site. The earlier phosphorylation at Ser727 was induced by UVB rather than UVC in keratinocytes, whereas the enhanced phosphorylation at Ser727 was not seen in the UVC-irradiated keratinocytes even under the ROS-sensitive condition using BSO. The timing of the UVB-induced p-Ser727 upregulation in the LA-treated cells was similar to UVC-induced Stat3 activation. Therefore, the phosphorylation at Ser727 seems to be mediated by both DNA damage and ROS. On the other hand, the phosphorylation at Tyr705 seems to be evoked mainly by ROS, which is yielded by UVB but not substantially by UVC. In this scenario, the upregulation by ROS may precede that by DNA damage on the Stat3 activation, which is consistent with our findings that Ser727 follows Tyr705 in the phosphorylation. Considering that precursors of ROS exist ubiquitously in cells, it appears that influence of ROS responded earlier than that of DNA damage in the phosphorylation. The delayed phosphorylation with H_2O_2 may be attributed to the difference between the extra- and intracellular ROS. In comparison with ROS, DNA damage induces the delayed phosphorylation presumably because of the indirect signalling pathway for the Stat3 activation.

While normal fibroblast showed little Stat3 upregulation by UVB and UVC irradiation at the same doses that HEK does, the upregulation of phospho-Stat3 protein by UV was seen in a dose-dependent manner in fibroblasts from a XP-A patient. To ask whether (i) the different responses in UV-induced Stat3 phosphorylation between normal and XP-A fibroblasts are attributed to the different abilities of DNA repair and (ii) the resultant difference in the amount of DNA damage in XP-A cells, XP-A fibroblasts were transfected with the *XPA* gene. XP1MG transfected with pcHA-*XPA* showed much lower responses to UVB and UVC in the Stat3 phosphorylation than XP1MG cells transfected with control vector, pcDNA3. The study using the transfected XP-A cells also supports the finding that Stat3 activation is induced by UVB *via* ROS and DNA damage and UVC largely *via* DNA damage. Stat3 activation operates upon cell proliferation to survive cellular damage under physiological UVB exposure, whereas deactivation of Stat3 through a rapid dephosphorylation of Tyr705 results in downregulation of anti-apoptotic molecules such as Bcl-xL

following excess UVB irradiation (9,24). Our data presented here are consistent with these findings.

Stat3 DNA binding activity is declined by 1000 J/m^2 of UVB exposure, which clinically evokes sunburn on human skin. Presumably, it is a self-defensive mechanism to eliminate the severely damaged cells by downregulating the anti-apoptotic pathway. Stat3 appears to promote cells to apoptosis in a way similar to that of tumor suppressor gene, p53 (25). Previously, we have demonstrated the downregulation of anti-apoptotic genes such as Bcl-2 or Bcl-xL by inhibition of Stat3 activation using RNA interference (9). Knezevic et al. have indicated the new UVB-induced signalling pathways to Bcl-2 of DNA photoproducts (e.g. cyclobutane pyrimidine dimer), which is an indirect and smaller component of the UV response than that of the P53-E2f1 pathway (25). Similarly, a new pathway mediated by DNA damage may play a critical role for Stat3 activation as a key regulator of UV responsiveness.

It has been shown that Stat3 activation contributes to biological activities, such as survival and maintenance of homeostasis (8). As Stat3 plays a pivotal role in cell proliferation and migration, it upregulates human telomerase reverse transcriptase (TERT) expression in both normal and tumor cells (26). An anti-ageing effect through TERT activity was observed under a cancer-resistant condition (27). Recently UV-induced skin ageing has been particularly reviewed from various viewpoints (28). Our observations in this study also suggest that Stat3 activation is one of the physiological responses to recover the photoageing in the senescence. The study of the mechanism of Stat3 activation could be helpful for a better understanding of the UV-induced skin ageing.

This study suggests that Stat3 activation in UV-exposed human skin is one of the initial events where DNA damage and ROS are involved and implies that Stat3 plays a critical role in the induction of apoptosis or senescence in response to UV. These findings regarding Stat3 may provide strategies to prevent photocarcinogenesis and photoageing.

Acknowledgements

This work was supported in part by Grants-in-Aid from the Ministry of Education, Culture, Sports, Science and Technology, Japan. We thank Mikuni Horie and Mio Hayashi for their excellent technical support.

Conflict of interest

The authors state no conflict of interest.

References

1 Fisher G J, Kang S, Varani J *et al.* Mechanisms of photoaging and chronological skin aging. Arch Dermatol 2002: **138**: 1462–1470.
2 Ahsan H, Aziz M H, Ahmad N. Ultraviolet B exposure activates Stat3 signaling via phosphorylation at tyrosine705 in skin of SKH1 hairless mouse: a target for the management of skin cancer? Biochem Biophys Res Commun 2005: **333**: 241–246.
3 Shen Y, Devgan G, Darnell J E Jr, Bromberg J F. Constitutively activated Stat3 protects fibroblasts from serum withdrawal and UV-induced apoptosis and antagonizes the proapoptotic effects of activated Stat1. Proc Natl Acad Sci U S A 2001: **98**: 1543–1548.
4 Sano S, Chan K S, Kira M *et al.* Signal transducer and activator of transcription 3 is a key regulator of keratinocyte survival and proliferation following UV irradiation. Cancer Res 2005: **65**: 5720–5729.
5 Mora L B, Buettner R, Seigne J *et al.* Constitutive activation of Stat3 in human prostate tumors and cell lines: direct inhibition of Stat3 signaling induces apoptosis of prostate cancer cells. Cancer Res 2002: **62**: 6659–6666.
6 Murakami Y, Nakano S, Niho Y, Hamasaki N, Izuhara K. Constitutive activation of Jak-2 and Tyk-2 in a v-Src-transformed human gallbladder adenocarcinoma cell line. J Cell Physiol 1998: **175**: 220–228.
7 Kube D, Holtick U, Vockerodt M *et al.* STAT3 is constitutively activated in Hodgkin cell lines. Blood 2001: **98**: 762–770.
8 Bromberg J F, Wrzeszczynska M H, Devgan G *et al.* Stat3 as an oncogene. Cell 1999: **98**: 295–303.
9 Sumita N, Bito T, Nakajima K, Nishigori C. Stat3 activation is required for cell proliferation and tumorigenesis but not for cell viability in cutaneous squamous cell carcinoma cell lines. Exp Dermatol 2006: **15**: 291–299.
10 Nishigori C, Moriwaki S, Takebe H, Tanaka T, Imamura S. Gene alterations and clinical characteristics of xeroderma pigmentosum group A patients in Japan. Arch Dermatol 1994: **130**: 191–197.
11 Corsini E, Terzoli A, Bruccoleri A, Marinovich M, Galli C L. Induction of tumor necrosis factor-alpha *in vivo* by a skin irritant, tributyltin, through activation of transcription factors: its pharmacological modulation by anti-inflammatory drugs. J Invest Dermatol 1997: **108**: 892–896.
12 Roy S, Sen C K, Kobuchi H, Packer L. Antioxidant regulation of phorbol ester-induced adhesion of human Jurkat T-cells to endothelial cells. Free Radic Biol Med 1998: **25**: 229–241.
13 Herrling T, Jung K, Fuchs J. Measurements of UV-generated free radicals/reactive oxygen species (ROS) in skin. Spectrochim Acta A Mol Biomol Spectrosc 2006: **63**: 840–845.
14 Schraufstatter I U, Hinshaw D B, Hyslop P A, Spragg R G, Cochrane C G. Glutathione cycle activity and pyridine nucleotide levels in oxidant-induced injury of cells. J Clin Invest 1985: **76**: 1131–1139.
15 Kuraoka I, Morita E H, Saijo M *et al.* Identification of a damaged-DNA binding domain of the XPA protein. Mutat Res 1996: **362**: 87–95.
16 Grether-Beck S, Olaizola-Horn S, Schmitt H *et al.* Activation of transcription factor AP-2 mediates UVA radiation- and singlet oxygen-induced expression of the human intercellular adhesion molecule 1 gene. Proc Natl Acad Sci U S A 1996: **93**: 14586–14591.
17 Fisher G J, Talwar H S, Lin J *et al.* Retinoic acid inhibits induction of c-Jun protein by ultraviolet radiation that occurs subsequent to activation of mitogen-activated protein kinase pathways in human skin *in vivo*. J Clin Invest 1998: **101**: 1432–1440.
18 Simon M M, Aragane Y, Schwarz A, Luger T A, Schwarz T. UVB light induces nuclear factor kappa B (NF kappa B) activity independently from chromosomal DNA damage in cell-free cytosolic extracts. J Invest Dermatol 1994: **102**: 422–427.
19 Huang C, Zhang D, Li J, Tong Q, Stoner G D. Differential inhibition of UV-induced activation of NF kappa B and AP-1 by extracts from black raspberries, strawberries, and blueberries. Nutr Cancer 2007: **58**: 205–212.
20 Dhanalakshmi S, Mallikarjuna G U, Singh R P. Agarwal R. Dual efficacy of silibinin in protecting or enhancing ultraviolet B radiation-caused apoptosis in HaCaT human immortalized keratinocytes. Carcinogenesis 2004: **25**: 99–106.
21 Gao S P, Mark K G, Leslie K *et al.* Mutations in the EGFR kinase domain mediate STAT3 activation via IL-6 production in human lung adenocarcinomas. J Clin Invest 2007: **117**: 3846–3856.
22 Koch-Paiz C A, Amundson S A, Bittner M L, Meltzer P S, Fornace A J Jr. Functional genomics of UV radiation responses in human cells. Mutat Res 2004: **549**: 65–78.
23 Cadet J, Sage E, Douki T. Ultraviolet radiation-mediated damage to cellular DNA. Mutat Res 2005: **571**: 3–17.
24 Sano S, Chan K S, DiGiovanni J. Impact of Stat3 activation upon skin biology: a dichotomy of its role between homeostasis and diseases. J Dermatol Sci 2008: **50**: 1–14.
25 Knezevic D, Zhang W, Rochette P J, Brash D E. Bcl-2 is the target of a UV-inducible apoptosis switch and a node for UV signaling. Proc Natl Acad Sci U S A 2007: **104**: 11286–11291.
26 Konnikova L, Simeone M C, Kruger M M, Kotecki M, Cochran B H. Signal transducer and activator of transcription 3 (STAT3) regulates human telomerase reverse transcriptase (hTERT) expression in human cancer and primary cells. Cancer Res 2005: **65**: 6516–6520.
27 Tomas-Loba A, Flores I, Fernandez-Marcos P J *et al.* Telomerase reverse transcriptase delays aging in cancer-resistant mice. Cell 2008: **135**: 609–622.
28 Berneburg M, Trelles M, Friguet B *et al.* How best to halt and/or revert UV-induced skin ageing: strategies, facts and fiction. Exp Dermatol 2008: **17**: 228–240.

Journal of Dermatological Science 61 (2011) 7–13

Contents lists available at ScienceDirect

Journal of Dermatological Science

journal homepage: www.elsevier.com/jds

Review article

Epithelial–mesenchymal transition in the skin

Motonobu Nakamura [a,*], Yoshiki Tokura [b]

[a] Department of Dermatology, University of Occupational and Environmental Health, 1-1 Iseigaoka, Yahatanishi-ku, Kitakyushu 807-8555, Japan
[b] Department of Dermatology, Hamamatsu University School of Medicine, 1-20-1 Handayama, Higashi-ku, Hamamatsu 431-1192, Japan

ARTICLE INFO

Article history:
Received 5 October 2010
Received in revised form 24 November 2010
Accepted 25 November 2010

Keywords:
Epithelial–mesenchymal transition
Snail
SNAI1
Fibrosis
Wound healing
Systemic sclerosis

ABSTRACT

Epithelial–mesenchymal transition (EMT) plays important roles not only in the morphogenesis but also in wound repair, tissue fibrosis and cancer progression. Recently, regulatory mechanism of this process has been elaborately elucidated. EMT can be a new therapeutic target for treating skin ulcer, fibrosing alopecia, and malignant cutaneous cancers, including squamous cell carcinoma and melanoma.

Contents

1. Introduction 7
2. EMT in skin morphogenesis 8
3. EMT in skin tumors 8
   3.1. EMT in squamous cell carcinoma 8
   3.2. EMT in malignant melanoma 9
   3.3. EMT in extramammary Paget's disease 9
4. EMT in wound healing 9
5. EMT in skin fibrosis 9
   5.1. EMT in postmenopausal frontal fibrosing alopecia 9
   5.2. EMT in systemic sclerosis 10
6. Structure of EMT inducer, SNAI1, and its associated molecules 11
7. Regulation of EMT 11
8. Conclusion 12
   References 12

1. Introduction

Epithelial–mesenchymal transition (EMT) is an intricate process by which epithelial cells lose their epithelial characteristics and acquire a mesenchymal-like phenotype. This dramatic phenotypic change involves the loss of E-cadherin (CDH1)-mediated cell–cell adhesion and prototypic epithelial marker expression, as well as the loss of apical–basal polarity and the acquisition of a motile behavior and a profound reorganization of the cytoskeleton (Fig. 1). Downregulation of CDH1 is one of the essential hallmarks for EMT. As CDH1 plays a crucial role in epithelial homeostasis, its downregulation can lead to decreased expression and/or organization of additional epithelial markers, desmosomal proteins (plakoglobin, desmogleins and desmoplakins), tight junction proteins and cell polarity proteins. Concomitantly, increased expression of mesenchymal markers (e.g., vimentin and fibronectin) as well as extracellular matrix remodeling enzymes (i.e., matrix metalloproteinases) is observed together with profound actin cytoskeleton reorganization. Thus, complex molecular and cellular mechanisms underlie EMT [1,2].

EMT was initially described in early embryogenesis which requires a migration and transient dedifferentiation of embryonic epithelial cells, gastrulation and the migration of neural crest cells. EMT and its reverse process (mesenchymal–epithelial transition,

* Corresponding author. Tel.: +81 93 691 7445; fax: +81 93 691 0907.
E-mail address: motonaka@med.uoeh-u.ac.jp (M. Nakamura).

0923-1811/$36.00 © 2010 Japanese Society for Investigative Dermatology. Published by Elsevier Ireland Ltd. All rights reserved.
doi:10.1016/j.jdermsci.2010.11.015

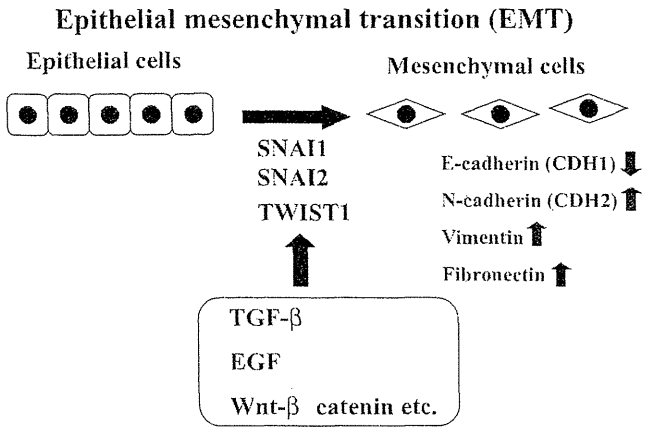

Fig. 1. Schematic model of epithelial–mesenchymal transition (EMT). Several factors, such as TGF-β, EGF and Wnt-β catenin signaling cascade, induce the expression of transcription factors, SNAI1, SNAI2 and TWIST1 in epithelial cells, which in turn led to the downregulation of E-cadherin (CDH1) expression, the upregulation of N-cadherin (CDH2), vimentin and fibronectin and the acquisition of morphological and functional features of mesenchymal cells.

MET) are indispensable for the differentiation and migration of specialized cell types and the acquisition of the complex three-dimensional structure of internal organs. However, EMT has recently been implicated to participate in tissue repair, cancer progression and organ fibrosis.

In this article, we review the current knowledge of EMT, focusing on its regulation in skin morphogenesis, wound repair, and cutaneous fibrosis, and discuss a future perspective of EMT-targeted therapeutics.

2. EMT in skin morphogenesis

EMT plays an important role in the gastrulation in the early development of vertebrates. Carver et al. studied embryos deficient for the Snail1 (*Snai1*), essential gene for EMT. *Snai1*$^{-/-}$ mice were embryonic lethal. At E6.5, *Snai1*$^{-/-}$ mutant embryos were indistinguishable from the embryos of heterozygous and wild-type littermates. At E7.5, however, the homozygous mutant embryos were smaller than the embryos of their littermates. By E8.5, the Snai1$^{-/-}$ embryos were severely retarded compared to those of littermates and were resorbed. At E7.5, Snai1$^{-/-}$ mutant mesoderm cells expressed mesoderm markers, however, they failed to show the characteristic mesenchymal morphology and had an appearance of a columnar epithelium. *Cdh1* expression was not downregulated in the Snai1$^{-/-}$ mutant mesoderm cells, while it was decreased in those in the littermates [3].

To examine EMT in skin morphogenesis, Kong et al. performed an immunohistochemical study with antibodies against Cdh1, α-smooth muscle (α-SMA), and fibronectin using mouse skin sections. They showed that cells expressing epithelial markers, Cdh1, zonula occludens 1 protein (ZO-1) and occludin were present in the dermal area during skin development with the highest expression from P2 to P5. The co-expression of an epithelial marker, Cdh1, and a mesenchymal marker, α-SMA, was observed in the dermis around P3–P6, suggesting some dermal cells might have developed through EMT [4].

Snai1 mRNA and protein are expressed transiently at the hair bud stage of hair follicle morphogenesis in mice. In contrast, Franci et al. detected Snai1 expression only in mesenchymal cells of the skin, particularly in the mesenchymal cells clustered below the hair buds of embryonic skin and in the dermal papillae of adult hair follicles. The discrepancy between the two studies has not been resolved [5,6].

Snai1 expression leads to the transcriptional downregulation of *Cdh1*, which results in junctional remodeling and bud formation. Transforming growth factor (TGF)-β2 is necessary to transiently induce Snai1 and activate the Ras-mitogen-activated protein kinase (MAPK) pathway in the bud [5].

Snai1 misexpression under the keratin 14 promoter in the epidermis of the transgenic mice led to a downregulation of Cdh1 and α-catenin, along with epidermal hyperproliferation and a reduction in an intercellular adhesion [5].

Slug (SNAI2) is another member of the Snail zinc-finger transcription factor family that plays crucial roles in EMT. Although *Snai1* expression is essential for normal embryonic development in mice, *Snai2*-null embryos are viable. Snai2$^{-/-}$ mice were small and had a diluted coat with the characteristic white forehead blaze. The histological sections of testis from Snai2$^{-/-}$ mice revealed testicular atrophy and a reduced number of Leydig cells. Moreover, Snai2$^{-/-}$ mice suffered from severe anemia. The activation of c-kit by stem cell factor (SCF) specifically induced *Snai2* expression, and Kit^{+} cells derived from *Snai2*$^{-/-}$ mice exhibited migratory defects. In this context, the human piebaldisms cases provide an interesting finding. Southern blot analysis revealed that 3 patients had evident heterozygous deletions of the *SNAI2* gene encompassing the entire coding region out of 17 unrelated patients with piebaldism, who lack apparent *KIT* mutations [7–9].

At the beginning of periderm formation at E12, Snai2 was expressed in essentially all skin epithelial cells and in the underlying mesenchyme. Snai2 staining was observed in progressively fewer dermal cells as primitive mesenchymal cells matured. In the placode, hair germ, and peg stages of hair follicle development, Snai2 expression was prominent in the thickened and invaginating epithelium but was absent from the underlying mesenchymal cells that ultimately form the dermal papillae [10].

In adult mice, Snai2-expressing keratinocytes were clustered around hair follicles. In developing follicles, Snai2 was stably expressed in the outer root sheath, hair matrix cells and some dermal papilla cells.

3. EMT in skin tumors

3.1. EMT in squamous cell carcinoma

Recently, we reported a case of squamous cell carcinoma that mimicked atypical fibroxanthoma and expressed both vimentin and SNAI1. Atypical fibroxanthoma, first described by Helwig in 1963, typically takes place on the head and neck of the elderly patients as a solitary nodule that is often ulcerated. Histologically, atypical mitotic figures and multinucleated cells are commonly seen in this tumor seemingly originating from mesenchymal stromal cells. Squamous cell carcinoma occasionally mimics atypical fibroxanthoma and can express vimentin, a mesenchymal marker. EMT in spindle cell squamous cell carcinoma has been reported by another Japanese group [11–14].

Hoot et al. reported a role of transforming growth factor (TGF)-β-Smad2 signaling pathway in the formation and progression of squamous cell carcinoma. Mice with keratinocyte-specific Smad2 deletion exhibited an accelerated formation and malignant progression of chemically induced squamous cell carcinomas compared with wild-type mice. Moreover, they revealed that the lack of SMAD2 expression in human squamous cell carcinoma was associated with reduced expression of CDH1, higher expression of SNAI1 and poor differentiation, indicating the involvement of EMT [15].

Regulation of TP63 isoforms may be one of the targets of SNAI1 and SNAI2 in cervical squamous cell carcinoma. *TP63* is a *TP53*-related gene that contains two alternative promoters, which give rise to transcripts that encode proteins with (TAp63) or without

(ΔNp63) an amino-transactivating domain. The expression of ΔN and TAp63 isoforms was down- and up-regulated *in vitro* by both SNAI1 and SNAI2, respectively. In SCC tissues, ΔN and TAp63 isoform expressions were, respectively, reduced and increased, when displaying a high immunoreactivity for SNAI1 and/or SNAI2. ΔNp63 silencing reduced cell–cell adhesion and increased the migratory properties of cancer cells. Therefore, the regulation of TP63 by SNAI1 and SNAI2 may play an important role in SCC tumor progression.

Herfs et al. revealed the reduced density of $CD1a^+$ Langerhans cells and downregulation of cell-surface CDH1 in an epithelial metaplasia of the uterine cervix. Langerhans cells are intraepithelial dendritic cells that initiate immune responses against antigens, including tumor antigens, on both skin and mucosal surfaces. Langerhans cells *in vitro* adhered poorly to keratinocytes transfected with either SNAI1 or SNAI2 DNA. Therefore, downregulation of CDH1 in keratinocytes by TGF-β-SMAD–SNAI1 signaling pathway not only leads to the EMT, but also the local immunodeficiency with a reduced function of Langerhans cells [16,17].

3.2. EMT in malignant melanoma

To determine whether human melanoma cells have decreased levels of CDH1, Tang et al. examined several human malignant melanoma cell lines for CDH1 expression. Of nine melanoma cells lines studied, six showed negative staining and three (SK-MEL-1, SK-MEL2 and SK-MEL-28) showed positive staining. Of the three CDH1 expressing cell lines, only SK-MEL-1 had CDH1 at a level comparable to that of normal melanocytes, while SK-MEL2 and SK-MEL-28 had decreased CDH1 expression.

Poser et al. analyzed the expression level of SNAI1 in melanoma cell lines. Significant SNAI1 expression was found in all 8 melanoma cells lines which had a reduced CDH1 expression, whereas no SNAI1 expression was detected in primary human melanocytes. Transient transfection of a *SNAI1* expression plasmid into human primary melanocytes led to the significant downregulation of CDH1, whereas transient and stable transfection of an anti-sense *SNAI1* construct induced reexpression of CDH1 in melanoma cell lines [18,19].

To explore a regulatory system for *SNAI1* expression, Palmer et al. analyzed chromatin structural changes associated with *SNAI1* transcription in melanoma cells. A robust DNase hypersensitive site (HS) was found in the 3′ region of A375 melanoma cells, in which SNAI1 was highly expressed, but not in keratinocytes or primary melanocytes. A physical interaction between the 3′ enhancer and promoter was observed in *SNAI1*-expressing cells, demonstrating a direct role for the enhancer in *SNAI1* expression. This finding suggested that the *SNAI1* promoter is constitutively packaged in a poised chromatin structure that can be activated in melanoma cells by a tissue specific enhancer, which physically contacts the promoter [20].

3.3. EMT in extramammary Paget's disease

Hirakawa et al. performed an immunohistochemical study and revealed that EMT markers, N-cadherin (CDH2) and vimentin, were not expressed by Paget cells at the early stage of carcinoma *in situ*, but expressed in invasive extramammary Paget's disease. They also revealed that CDH2 and vimentin expressions in extramammary Paget's disease significantly correlated with reduced overall survival. Cytoplasmic CDH1 expression was detectable by the early stages of tumor progression in subpopulation of patients with a poor outcome. Kaplan–Meier analysis showed that cytoplasmic CDH1 was a prognostic factor for reduced overall survival in extramammary Paget's disease, indicating that EMT-like process plays a key role in promoting tumor invasion within the primary sites [21].

4. EMT in wound healing

Successful wound healing is a complex process involving cells of the epidermis, dermis, vasculture, and the immune system. Two distinct cellular mechanisms directly contribute to the closure of skin wounds: keratinocyte-driven reepithelialization, which is achieved through a combination of migration and reduced intercellular adhesion in the epidermis proximal to the wound margin, and fibroblast-mediated contraction of the newly formed connective tissue bed beneath the wound site, pulling the edges of the wound closer together [22].

The migratory activity and the reduced intercellular adhesion of keratinocytes observed in reepithelialization recapitulate several aspects of EMT. Savagner et al. analyzed the expression of Snai2 during the wound healing by *in situ* hybridization. Snai2 expression was elevated in keratinocytes bordering cutaneous wounds in mice *in vivo*, in keratinocytes migrating from mouse skin explants *ex vivo*, and in human keratinocytes at wound margins *in vitro*. Epithelial cell outgrowth from skin explants of *Snai2* deficient mice was severely compromised. Overexpression of *Snai2* in keratinocytes caused increased cell spreading and desmosomal disruption. Moreover, *in vitro* wound healing was markedly accelerated in keratinocytes that ectopically expressed *Snai2*, suggesting a critical role for Snai2 in epithelial keratinocyte migration and wound healing [23].

The reepithelialization of excisional wound healing was significantly impaired in *Snai2* deficient mice. Furthermore, 8 out of 20 *Snai2* null mice but no wild type mice developed non-healing cutaneous ulcers in response to chronic UV irradiation. This knockout study also revealed an important role of Snai2 in modulating EMT in successful wound repair [24].

Epidermal growth factor (EGF) treatment of human keratinocytes induced activating phosphorylation of ERK5 and up-regulation of *SNAI2* transcription. Ectopic activation of ERK5 led to an increased *SNAI2* mRNA expression level and faster wound healing. In contrast, expression of shRNA specific for ERK5 in keratinocytes decreased *SNAI2* expression and motility response to EGF and led to an altered more compact morphology, along with disruption the of desmosome organization of keratinocytes. The results indicated an EGFR/ERK5/SNAI2 pathway in the control of EMT in wound healing by EGF [25,26].

5. EMT in skin fibrosis

5.1. EMT in postmenopausal frontal fibrosing alopecia

It had been thought that fibrosis is formed by the pathological activation of interstitial fibroblasts and the resultant conversion to myofibroblasts producing the fibrotic collagen network. In a renal fibrosis, however, elegant cell tracing studies have shown that a significant portion of these myofibroblasts arises from the conversion of epithelial cells through an EMT process [27].

Moreover, Kim et al. revealed that EMT also takes place during the development of pulmonary fibrosis. To examine the capacity of alveolar epithelial cells for EMT, they generated mice expressing β-galactosidase (β-gal) exclusively in lung epithelial cells. In an established model of pulmonary fibrosis, overexpression of active TGF-β1, β-gal-positive cells expressing mesenchymal markers accumulated. The increase in vimentin-positive cells within lungs was nearly all β-gal-positive, indicating epithelial cells as the main source of mesenchymal expansion in this model. *Ex vivo*, primary alveolar epithelial cells cultured on provisional matrix compo-

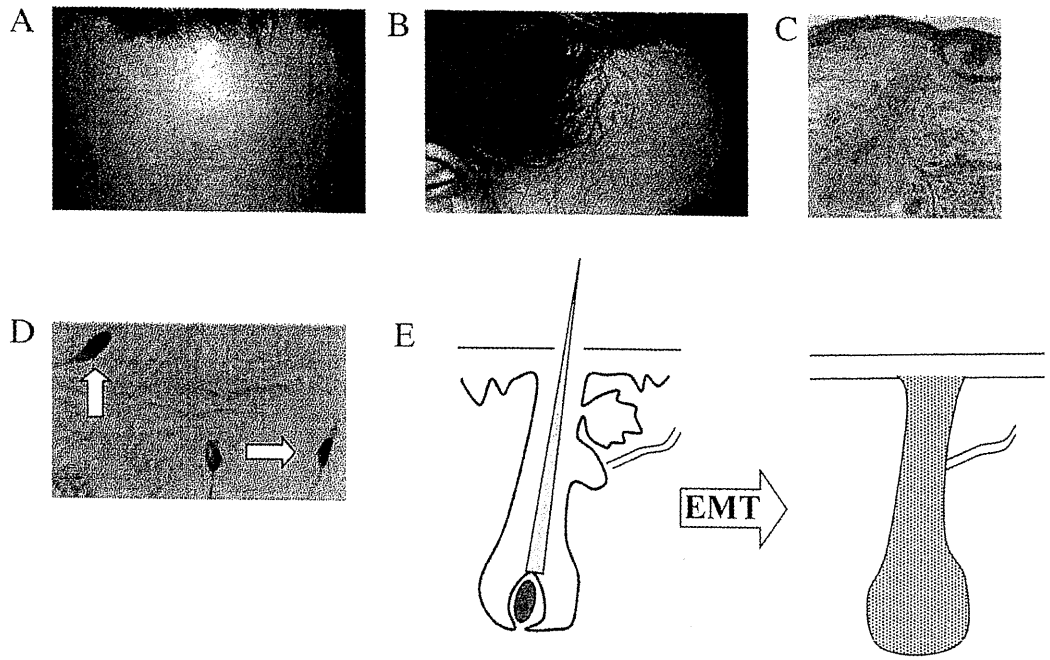

Fig. 2. (A and B) Frontotemporal recession with uniformly pale skin in a postmenopausal frontal fibrosing alopecia patient. (C) Histology of a biopsy specimen taken from the temporal region of the patient. An arrector pili muscle inserting into the fibrotic tissue surrounded by sparse lymphocytes. (D) SNAI1 positive cells found in the fibrotic dermis (arrows). (E) Proposed schematic formation of postmenopausal frontal fibrosing alopecia. EMT in hair follicles leads to the fibrosing alopecia.

nents, fibronectin or fibrin, underwent robust EMT *via* integrin-dependent activation of endogenous latent TGF-β1 [28].

Postmenopausal frontal fibrosing alopecia is characterized by a progressive frontoptemporal recession due to a scarring hair loss. Histological examination shows a reduction or loss of terminal hair follicles and a replacement by fibrosis around the affected hair follicles. Lymphocytic infiltration is usually observed in a lichenoid pattern in the upper dermis. Altal frontal fibrosing alopecia is considered as a variant of lichen planopilaris, its exact pathogenesis still remains to be clarified [29,30].

We reported a case of postmenopausal frontal fibrosing alopecia showing the expression of SNAI1 in the fibrotic dermis, suggesting a role of EMT in the pathogenesis (Fig. 2A–D). The existence of SNAI1 positive cells in the fibrotic dermis of our case suggested that the fibroblasts are in part derived from the hair-follicle cells *via* an EMT process (Fig. 2E). SNAI1 up-regulates several chemokines which may play a role in lichenoid reaction in frontal fibrosing alopecia [31].

5.2. EMT in systemic sclerosis

Systemic sclerosis (SSc) is an autoimmune disorder characterized by extensive fibrosis associated with collagen synthesis increased by the myofibroblasts and its accumulation. There are a wide variety of hypothesis on the origin of myofibroblasts in SSc patients. Postlethwaite et al. suggested that conventional, circu-

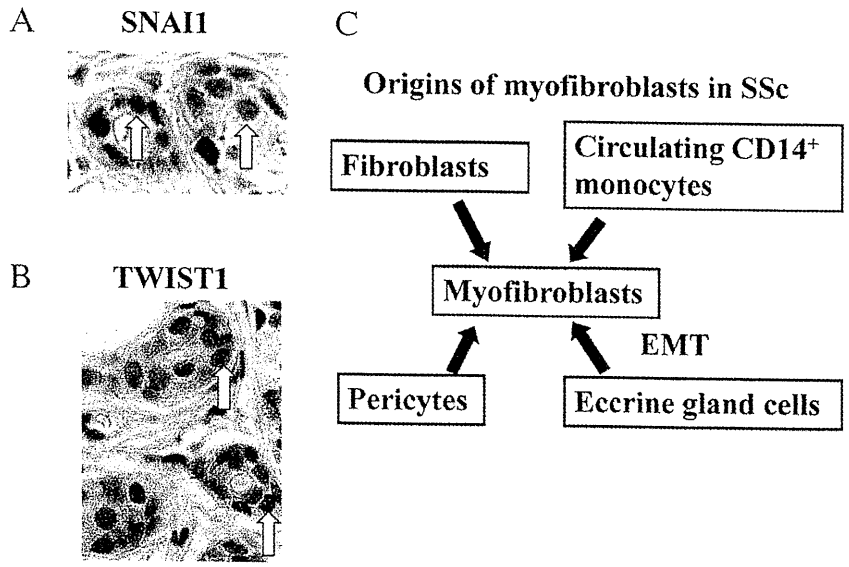

Fig. 3. (A) Expression of SNAI1 in the eccrine glands in a systemic sclerosis patient (arrows). (B) Expression of TWIST1 in the eccrine glands in a systemic sclerosis patient (arrows). (C) Several hypotheses on the origin of myofibroblasts which play central roles in the pathogenesis of systemic sclerosis (SSc). Myofibroblasts have been proposed to be derived from fibroblasts, circulating $CD14^+$ monocytes, pericytes and eccrine gland cells.

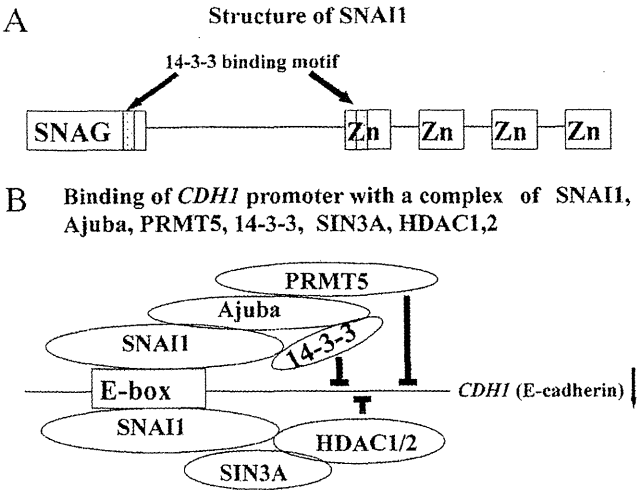

Fig. 4. (A) Structure of SNAI1. SNAI1 contains an NH_2-terminal SNAG (Snail/Slug and Gfi-1) repression domain and COOH-four COOH-terminal tandem C_2–H_2 zinc finger motifs. (B) SNAI1 binds to the E-box of *CDH1* promoter with zinc finger motifs. SNAI1 is associated with other proteins and forms a multiprotein complex.

lating $CD14^+$ monocytes transdifferentiate into SSc myofibroblasts. Another group postulated a link between vascular damage and the formation of myofibroblasts from pericytes in SSc. Pericytes are primitive mesenchymal cells and can differentiate into myofibroblasts, cartilage and bones [32,33].

To examine the expression of EMT markers in the skin of three SSc female patients, we performed an immunohistochemistry against forearm skin specimens using antibodies against EMT markers, SNAI1 and TWIST1. Both SNAI1 and TWIST1 expressions were observed in the eccrine glands (Fig. 3A and B) in each dSSc patient. Neither SNAI1 nor TWIST1 expression was observed in two age-matched females' skins. These results suggested that SNAI1 and TWIST1 expression may be induced in eccrine glands at the early and/or progressive stage of dSSc. A part of the cells of eccrine glands, with a tissue-stem cell like character or not, might undergo EMT and differentiate into the myofibroblasts, contributing, at least partially, to the pathogenesis of SSc (Fig. 3C) [34,35].

6. Structure of EMT inducer, SNAI1, and its associated molecules

The SNAI1 protein contains an NH_2-terminal SNAG (Snail/Slug and Gfi-1) repression domain and COOH-four COOH-terminal tandem C_2–H_2 zinc finger motifs (Fig. 4A). SNAG motif was first identified as the growth factor independence-1 (*GFI-1*) proto-oncogene encoded protein. The SNAG domain comprises the first 21 amino acid residues in the N terminus, a potent and transferable repression motif.

Ayyanathan et al. searched SNAG domain-associated proteins by performing yeast two hybrid systems using SNAG domain as a bait. They identified Ajuba, a multiple LIM domain protein that can function as a corepressor for the SNAG domain. Ajuba interacts with the SNAG domain *in vitro* and *in vivo*, colocalizes with it, and enhances SNAG-mediated transcriptional repression (Fig. 4B) [36].

Moreover, the same group identified protein arginine methyltransferase 5 (PRMT5) as an effector recruited to SNAI1 through an interaction with AJUBA that functions to repress the SNAI1 target gene, *Cdh1*. PRMT5 binds to the non-LIM region of AJUBA and is translocated into the nucleus in a SNAI1- and AJUBA-dependent manner. The depletion of PRMT5 promotes Cdh1 expression [37].

Hou et al. also defined functional 14-3-3 binding motifs in SNAI1 and AJUBA, which selectively bind 14-3-3 isoforms. In SNAI1, an NH_2-terminal motif in the SNAG domain cooperates with a COOH-terminal high-affinity motif for binding to 14-3-3 proteins (Fig. 4A). Coordinate mutation of both motifs abolishes 14-3-3 binding and inhibits SNAI-mediated gene repression and EMT differentiation. SNAI1, 14-3-3 proteins, and Ajuba form a ternary complex that is detected through chromatin immunoprecipitation at the endogenous Cdh1 promoter [38].

Snai1 is also associated with histone deacetylase 1 (HDAC1) and HDAC2, and the corepressor Sin3A through the SNAG domain of Snai1. Snai1 requires HDAC activity to repress Cdh1 promoter and overexpression of Snai1 is correlated with deacetylation of histones H3 and H4 (Fig. 4B). Thus Snai1 repressed Cdh1 by the recruitment of chromatin remodeling and histone modifying activities [39].

7. Regulation of EMT

EMT is controlled by various factors through both transcriptional and post-transcriptional ways. The regulation of EMT was excellently reviewed by Peinado et al. EMT is induced by TGF-β-bone morphogenetic protein (BMP)-SMAD pathway, Wnt-β catenin signaling, and receptor tyrosine kinases (RTKs). RTKs are activated by different signals, such as fibroblast growth factor (FGF), platelet derived growth factor (PDGF) and epidermal growth factor (EGF) (Table 1). Comparative analysis of *SNAI1* and *SNAI2* promoters from different species has identified conserved and functional response elements, such as AP1 and AP4 sites, SMAD-binding elements, LEF1 binding sites and two conserved E-boxes. SNAI1 or Snai1 expression is also controlled by a mucin, *Helicobacter pylori* infection, a zinc-finger transcription factor, Wilms' tumor-1 (Wt1), polycomb group protein B lymphoma Mo-MLV insertion region 1 homolog (Bmi-1), and phosphoinositide-dependent protein kinase (PDK) 1. SNAI1 is also regulated posttranscriptionally through ubiquitination and degrading processes by molecules, such as GSK3β and CK1ε. In the following sections, we focus on recent findings on EMT inducers and repressors [40–48].

Recently several lines of evidence have shown that sex hormones, androgens and estrogens, play crucial roles in mediating EMT processes. Androgens exert their biological effects by binding to the androgen receptor and inducing its transcriptional activity. Androgens induced the EMT pattern in prostate tumor epithelial cell with SNAI1 activation and lead to significant changes in prostate cancer cell migration and invasion potential. Expression levels of androgen receptors inversely correlated with androgen-mediated EMT in prostate tumor epithelial cells, pointing to a low androgen receptor content required for the EMT phenotype. On the contrary, estrogen receptor β plays an important role in maintaining an epithelial phenotype and repressing mesenchymal characteristics in prostate carcinoma. Poorly differentiated tumors exhibit diminished estrogen receptor

Table 1
Summary of reported inducers and repressor of EMT.

Inducer	Repressor
Androgen	Estrogen-ERβ
Estrogen-ERα	GSK3
TGF-β1, Wnt-β catenin	CK1
Helicobacter pylori	
MUC4 mucin, EGF	
Wilms' tumor 1 (Wt1)	
Bmi-1	
Hypoxia-HIF	
VEGF, FGF, PDGF	
RAS-MAPK	

β expression. Loss of estrogen receptor β is sufficient to promote an EMT [49,50].

The estrogen receptor α signaling plays an important role in human breast cancer formation and progression. Human breast cancers exhibit a strong direct correlation between estrogen receptor α and CDH1 expression by immunohistochemistry. When estrogen receptor α was knocked down in the estrogen receptor α positive cell lines, SNAI2 increased, CDH1 decreased, and cells became spindly and exhibited increased Matrigel invasion. When estrogen receptor α was overexpressed in the estrogen receptor α-negative cell lines, 17β-estradiol decreased SNAI2 and increased CDH1 expression, and decreased invasiveness of tumor cells in Matrigel [51].

8. Conclusion

In this review, we focused on the important roles of EMT in wound healing, tumor formation and cutaneous fibrosis. In addition, we reviewed the recent findings on the regulation of EMT by various factors. The concept of EMT has been widely accepted just for a decade, and there may remain other skin diseases in which EMT plays a crucial role in the pathogenesis. Appropriate control of EMT in the skin by the modulation of EMT inducers and repressors can be a new therapeutic target in future for skin diseases, including skin ulcer, cutaneous malignant tumors and systemic fibrosis.

References

[1] Thiery JP, Acloque H, Huang RYJ, Nieto MA. Epithelial–mesenchymal transitions in development and disease. Cell 2009;139:871–90.
[2] Morneo-Bueno G, Peinado H, Molina P, Olmeda D, Cubillo E, Santos V, et al. The morphological and molecular features of the epithelial-to-mesenchymal transition. Nat Protocol 2009;4:1591–613.
[3] Carver EA, Jiang R, Lan Y, Oram KF, Gridley T. The mouse Snail gene encodes a key regulator of the epithelial–mesenchymal transition. Mol Cell Biol 2001;21:8184–8.
[4] Kong W, Li S, Liu C, Bari AS, Longaker MT, Lorenz HP. Epithelial–mesenchymal transition occurs after epidermal development in mouse skin. Exp Cell Res 2006;312:3959–68.
[5] Jamora C, Lee P, Kocieniewski P, Azhar M, Hosokawa R, Chai Y, et al. A signaling pathway involving TGF-β2 and Snail in hair follicle morphogenesis. PLoS Biol 2005;3:e11.
[6] Franci C, Takkunen M, Dave N, Alameda F, Gomez S, Rodriguez R, et al. Expression of Snail protein in tumor–stroma interface. Oncogene 2006;25:5134–44.
[7] Jiang R, Lan Y, Norton CR, Sundberg JP, Gridley T. The Slug gene is not essential for mesoderm or neural crest development in mice. Dev Biol 1998;198:277–85.
[8] Perez-Losada J, Sanchez-Martin M, Rodriguez-Garcia A, Sanchez ML, Orfao A, Flores T, et al. Zinc-finger transcription factor Slug contributes to the function of the stem cell factor c-kit signaling pathway. Blood 2002;199:1274–86.
[9] Sanchez-Martin M, Perez-Losada J, Rodriguez-Garcia A, Gonzalez-Sanchez B, Korf BR, Kuster W, et al. Deletion of the SLUG (SNAI2) gene results in human piebaldism. Am J Med Genet A 2003;122A:125–32.
[10] Parent AE, Newkirk KM, Kusewitt DF. Slug (Snai2) expression during skin and hair follicle development. J Invest Dermatol 2010;130:1737–9.
[11] Nakamura M, Sugita K, Tokura Y. Expression of Snail1 in the vimentin-expressing squamous cell carcinoma mimicking atypical fibroxanthoma: possible involvement of an epithelial–mesenchymal transition. J Eur Acad Dermatol Venereol 2010;24:1365–6.
[12] Helwig EB. Atypical fibroxanthoma. Tex J Med 1963;59:664–7.
[13] Gray Y, Robidoux HJ, Farrell DS, Robinson-Bostom L. Squamous cell carcinoma detected by high-molecular-weight cytokeratin immunostaining mimicking atypical fibroxanthoma. Arch Pathol Lab Med 2001;125:799–802.
[14] Iwata H, Aoyama Y, Kamiya H, Ichiki Y, Kitajima Y. Spindle cell squamous cell carcinoma showing epithelial–mesenchymal transition. J Eur Acad Dermatol 2009;23:214–5.
[15] Hoot KE, Lighthall J, Han G, Lu SL, Li A, Ju W, et al. Keratinocyte-specific Smad2 ablation results in increased epithelial–mesenchymal transition during skin cancer formation and progression. J Clin Invest 2008;118:2722–32.
[16] Herfs M, Hubert P, Suarez-Carmona M, Reschner A, Saussez S, Berx G, et al. Regulation of p63 isoforms by Snail and Slug transcription factors in human squamous cell carcinoma. Am J Pathol 2010;176:1941–9.
[17] Herfs M, Hubert P, Kholod N, Caberg JH, Gilles C, Berx G, et al. Transforming growth factor-β1-mediated Slug and Snail transcription factor up-regulation reduces the density of Langerhans cells in epithelial metaplasia by affecting E-cadherin expression. Am J Pathol 2008;172:1391–402.
[18] Tang A, Eller MS, Hara M, Yaar M, Hirohashi S, Gilchrest BA. E-cadherin is the major mediator of human melanocyte adhesion to keratinocytes in vitro. J Cell Sci 1994;107:983–92.
[19] Poser I, Dominguez D, de Herreros AG, Varnai A, Buettner R, Bosserhoff AK. Loss of E-cadherin expression in melanoma cells involves up-regulation of the transcriptional repressor Snail. J Biol Chem 2001;276:24661–6.
[20] Palmer MB, Majumder P, Green MR, Wade PA, Boss JM. A 3′ enhancer controls Snail expression in melanoma cells. Cancer Res 2007;67:6113–20.
[21] Hirakawa S, Detmar M, Kerjaschki D, Nagamatsu S, Matsuo K, Tanemura A, et al. Nodal lymphangiogenesis and metastasis. Role of tumor-induced lymphatic vessel activation in extramammary Paget's disease. Am J Pathol 2009;175:2235–48.
[22] Coulombe PA. Wound epithelialization: accelerating the pace of discovery. J Invest Dermatol 2003;121:219–30.
[23] Savagner P, Kusewitt DF, Carver EA, Magnino F, Choi C, Gridley T, et al. Developmental transcription factor Slug is required for effective re-epithelialization by adult keratinocytes. J Cell Physiol 2005;202:858–66.
[24] Hudson LG, Newkirk KM, Chandler HL, Choi C, Fossey SL, Parent AE, et al. Cutaneous wound reepithelialization is compromised in mice lacking functional Slug (Snai2). J Dermatol Sci 2009;56:19–26.
[25] Arnoux V, Nassour M, L'Helgoualc'h A, Hipskind RA, Savagner P. Erk5 controls Slug expression and keratinocyte activation during wound healing. Mol Biol Cell 2008;19:4738–49.
[26] Kusewitt DF, Choi C, Newkirk KM, Leroy P, Li Y, Chavez MG, et al. Slug/Snai2 is a downstream mediator of epidermal growth factor receptor-stimulated reepithelialization. J Invest Dermatol 2009;129:491–5.
[27] Iwano M, Plieth D, Danoff TM, Xue C, Okada H, Neilson EG. Evidence that fibroblasts derive from epithelium during tissue fibrosis. J Clin Invest 2002;110:341–50.
[28] Kim KK, Kugler MC, Wolters PJ, Robillard L, Galvez MG, Brumwell AN, et al. Alveolar epithelial cell mesenchymal transition develops *in vivo* during pulmonary fibrosis and is regulated by the extracellular matrix. Proc Natl Acad Sci USA 2006;103:13180–5.
[29] Kossard S. Postmenopausal frontal fibrosing alopecia. Arch Dermatol 1994;130:770–4.
[30] Tan KT, Messenger AG. Frontal fibrosing alopecia: clinical presentations and prognosis. Br J Dermatol 2009;160:75–9.
[31] Nakamura M, Tokura Y. Expression of Snail1 in the fibrotic dermis of postmenopausal frontal fibrosing alopecia: possible involvement of an epithelial–mesenchymal transition and a review of the Japanese patients. Br J Dermatol 2010;162:1152–4.
[32] Postlethwaite AE, Shigemitsu H, Kanangat S. Cellular origins of fibroblasts: possible implications for organ fibrosis in systemic sclerosis. Curr Opin Rheumatol 2004;16:733–8.
[33] Rajkumar VS, Howell K, Csiszar K, Denton CP, Black CM, Abraham DJ. Shared expression of phenotypic markers in systemic sclerosis indicated a convergence of pericytes and fibroblasts to a myofibroblast lineage in fibrosis. Arth Res Ther 2004;7:R1113–2.
[34] Nakamura M, Tokura Y. Expression of SNAI1 and TWIST1 in the eccrine glands of systemic sclerosis patients: possible involvement of epithelial–mesenchymal transition in the pathogenesis. Br J Dermatol, in press, doi:10.1111/j.1365-2133.2010.10021.x.
[35] Nakamura M, Tokura Y. The localization of label-retaining cells in eccrine glands. J Invest Dermatol 2009;129:2077–8.
[36] Ayyanathan K, Peng H, Hou Z, Fredericks WJ, Goyal RK, Langer EM, et al. The Ajuba LIM domain protein is a corepressor for SNAG domain-mediated repression and participates in nucleocytoplasmic shuttling. Cancer Res 2007;67:9097–106.
[37] Hou Z, Peng H, Ayyanathan K, Yan KP, Langer EM, Longmore GD, et al. The LIM protein AJUBA recruits protein arginine methyltransferase 5 to mediate SNAIL-dependent transcriptional repression. Mol Cell Biol 2008;28:3198–207.
[38] Hou Z, Peng H, White DE, Wang P, Lieberman PM, Halazonetis T, et al. 14-3-3 binding sites in the Snail protein are essential for Snail-mediated transcriptional repression and epithelial–mesenchymal differentiation. Cancer Res 2010;70:4385–93.
[39] Peinado H, Ballestar E, Esteller M, Cano A. Snail mediates E-cadherin repression by the recruitment of the Sin3A/histone deacetylase 1 (HDAC1)/HDAC2 complex. Mol Cell Biol 2004;24:306–19.
[40] Peinado H, Olmeda D, Cano A. Snail ZEB and bHLH factors in tumour progression: an alliance against the epithelial phenotype? Nat Rev Cancer 2007;7:415–28.
[41] De Craene B, van Roy F, Berx G. Unraveling signaling cascades for the Snail family of transcription factors. Cell Signal 2005;17:535–47.
[42] Yin Y, Grabowka AM, Clarke PA, Whelband E, Robinson K, Argent RH, et al. *Helicobacter pylori* potentiates epithelial:mesenchymal transition in gastric cancer: links to soluble HB-EGF, gastrin and matrix metalloproteinase-7. Gut 2010;59:1037–45.
[43] Ponnusamy MP, Lakshmanan I, Jain M, Das S, Chakraborty S, Dey P, et al. MUC4 mucin-induced epithelial to mesenchymal transition: a novel mechanism for metastasis of human ovarian cancer cells. Oncogene 2010. doi: 10.1038/onc.2010.309.
[44] Martinez-Estrada OM, Latiice LA, Essafi A, Guadix JA, Slight J, Velecela V, et al. Wt1 is required for cardiovascular progenitor cell formation through transcriptional control of Snail and E-cadherin. Nat Genet 2010;42:89–94.
[45] Song LB, Li J, Liao WT, Feng Y, Yu CP, Hu LJ, et al. The polycomb group protein Bmi-1 represses the tumor suppressor PTEN and induces epithelial–mesenchymal transition in human nasopharyngeal epithelial cells. J Clin Invest 2009;119:3626–36.

[46] Feng Q, Di R, Tao F, Chang Z, Lu S, Fan W, et al. PDK1 regulates vascular remodeling and promotes epithelial–mesenchymal transition in cardiac development. Mol Cell Biol 2010;30:3711–21.
[47] Zhou BP, Deng J, Xia W, Xu J, Li YM, Gunduz M, et al. Dual regulation of Snail by GSK-3β-mediated phosphorylation in control of epithelial–mesenchymal transition. Nat Cell Biol 2004;6:931–40.
[48] Xu Y, Lee SH, Kim HS, Piao S, Park SH, Jung YS, et al. Role of CK1 in GSK-3β-mediated phosphorylation and degradation of Snail. Oncogene 2010;29: 3124–33.
[49] Zhu ML, Kyprianou N. Role of androgens and the androgen receptor in epithelial–mesenchymal transition and invasion of prostate cancer cells. FASEB J 2010;24:769–77.
[50] Mak P, Leav I, Pursell B, Bae D, Yang X, Taglienti CA, et al. ERβ impedes prostate cancer EMT by destabilizing HIF-1α and inhibiting VEGF-mediated Snail nuclear localization: implications for Gleason grading. Cancer Cell 2010;17: 319–32.
[51] Ye Y, Xiao Y, Wang W, Yearsley K, Gao JX, Shetuni B, et al. ERα signaling through slug regulates E-cadherin and EMT. Oncogene 2010;29:1451–62.

ORIGINAL ARTICLE

Topical Cholecystokinin Depresses Itch-Associated Scratching Behavior in Mice

Shoko Fukamachi[1], Tomoko Mori[1], Jun-Ichi Sakabe[1], Noriko Shiraishi[1], Etsushi Kuroda[2], Miwa Kobayashi[1], Toshinori Bito[3], Kenji Kabashima[4], Motonobu Nakamura[1] and Yoshiki Tokura[1,5]

Cholecystokinin (CCK) serves as a gastrointestinal hormone and also functions as a neuropeptide in the central nervous system (CNS). CCK may be a downregulator in the CNS, as represented by its anti-opioid properties. The existence of CCK in the peripheral nervous system has also been reported. We investigated the suppressive effects of various CCKs on peripheral pruritus in mice. The clipped backs of ICR mice were painted with CCK synthetic peptides and injected intradermally with substance P (SP). The frequency of SP-induced scratching was reduced significantly by topical application of sulfated CCK8 (CCK8S) and CCK7 (CCK7S), but not by nonsulfated CCK8, CCK7, or CCK6. Dermal injection of CCK8S also suppressed the scratching frequency, suggesting that dermal cells as well as epidermal keratinocytes (KCs) are the targets of CCKs. As determined using real-time PCR, mRNA for CCK2R, one of the two types of CCK receptors, was expressed highly in mouse fetal skin-derived mast cells (FSMCs) and moderately in ICR mouse KCs. CCK8S decreased *in vitro* compound 48/80-promoted degranulation of FSMCs with a transient elevation of the intracellular calcium concentration. These findings suggest that CCK may exert an antipruritic effect via mast cells and that topical CCK may be clinically useful for pruritic skin disorders.

Journal of Investigative Dermatology advance online publication, 3 February 2011; doi:10.1038/jid.2010.413

INTRODUCTION

Itch or pruritus is an unpleasant cutaneous sensation associated with the immediate desire to scratch (Ikoma *et al.*, 2006; Steinhoff *et al.*, 2006). Histamine was long considered the only mediator of pruritus, but this assumption has changed dramatically in the past two decades. Peripheral itch can be evoked in the skin either directly, by mechanical and thermal stimuli, or indirectly, through chemical mediators (Ikoma *et al.*, 2006). Itch may also be generated in the central nervous system (CNS) independent of peripheral stimulation. Different puritic diseases involved different itch mediators, including histamine, neuropeptides, proteases, prostaglandins, serotonin, acetylcholine, cannabinoids, opioids, bradykinins, cytokines, biogenic amines, neurotransmitters, and ion channels (Steinhoff *et al.*, 2006).

Neuromediators such as neuropeptides and neurotrophins, as well as their receptors, have an important role in peripheral itch. Neuropeptides, as represented by pruritogenic neuropeptide substance P (SP), are produced by sensory nerves, but they can also be elaborated by epidermal keratinocytes (KCs), mast cells, fibroblasts, and other cutaneous immunocompetent cells (Ohkubo and Nakanishi, 1991; Scholzen *et al.*, 1998). Many other mediators are also produced by and secreted from skin-constituent cells in close contact to sensory nerves (Steinhoff *et al.*, 2006). They can activate and sensitize pruritic nerve endings and even modulate their growth, as do nerve growth factors and chemorepellents (Yamaguchi *et al.*, 2008; Yosipovitch and Papoiu, 2008). As for the receptor system, it is notable that KCs, mast cells, and fibroblasts express neurokinin-1 receptor (Ohkubo and Nakanishi, 1991; Scholzen *et al.*, 1998), which is the receptor for SP. These complicated neurophysiological interactions yield itch and render its therapeutic control difficult.

Cholecystokinin (CCK) is a peptide hormone in the gastrointestinal tract (Dufresne *et al.*, 2006), but it also serves as a neuropeptide (Ma *et al.*, 2006). Among neuropeptides, CCKs are most abundantly present in the CNS and involved in numerous physiological functions such as anxiety, depression, psychosis, memory, and feeding behavior (Dufresne *et al.*, 2006). CCKs also have anti-opioid properties in the CNS (Pommier *et al.*, 2002; Mollereau *et al.*, 2005) and exert a nociceptive effect in the spinal cord (Wiesenfeld-Hallin *et al.*, 1999). Furthermore, their existence in the peripheral nervous system has been reported (Moriarty *et al.*, 1997). In various CCKs, sulfation of the tyrosine at position 7

[1]*Department of Dermatology, University of Occupational and Environmental Health, Kitakyushu, Japan;* [2]*Department of Immunology, University of Occupational and Environmental Health, Kitakyushu, Japan;* [3]*Department of Dermatology, Kobe University, Kobe, Japan;* [4]*Department of Dermatology, Kyoto University Graduate School of Medicine, Kyoto, Japan and* [5]*Department of Dermatology, Hamamatsu University School of Medicine, Hamamatsu, Japan*

Correspondence: Yoshiki Tokura, Department of Dermatology, Hamamatsu University School of Medicine, 1-20-1 Handayama, Higashi-Ku, Hamamatsu 431-3192, Japan. E-mail: tokura@hama-med.ac.jp

Abbreviations: CCK, cholecystokinin; CCK2R, CCK2 receptor; CCK7S, sulfated CCK7; CCK8S, sulfated CCK8; CNS, central nervous system; FSMC, murine fetal skin-derived mast cell; KC, keratinocyte; SP, substance P

Received 15 February 2010; revised 3 November 2010; accepted 12 November 2010

from the C-terminus is a posttranslational modification that makes them biologically active peptides (Ma *et al.*, 2006). Varying lengths of CCKs with or without sulfate have been studied for their activities as gastrointestinal hormones (Bonetto *et al.*, 1999) and as CNS players (Rehfeld *et al.*, 2007). Two types of CCK receptors have been identified: CCK1R (CCK-A receptor) and CCK2R (CCK-B receptor). CCK1R usually requires sulfated CCKs. CCK2R affords a binding site to both sulfated and nonsulfated ligands, but nonsulfated CCKs have affinities that are decreased 10- to 50-fold (Dufresne *et al.*, 2006). CCKs exert their biological functions by interacting with CCK receptors located on multiple target cells in the CNS and on peripheral nerve endings (Dufresne *et al.*, 2006; Rehfeld *et al.*, 2007; Zheng *et al.*, 2009). In the brain, sulfated CCK8 (CCK8S) is most abundant (Rehfeld *et al.*, 2007) and possesses one of the strongest endogenous anti-opioid properties (Ma *et al.*, 2006). Prolonged opioid exposure increases the expression of CCKs and CCK2R in the CNS, where CCK8S negatively modulates opioid responses and maintains homeostasis of the opioid system (Pommier *et al.*, 2002; Agnes *et al.*, 2008). Thus, it seems that CCKs are downregulators of opioid-mediated pruritus in CNS. However, the function of CCKs, the distribution of CCK receptors in the skin, and their effects on peripheral pruritus remain unelucidated (Ma *et al.*, 2006).

In this study, we investigated the antipruritic effects of different lengths of CCKs with or without sulfate, which were topically applied onto the skin of mice. Results suggest that CCKs are capable of reducing SP-induced scratching at least by affecting the function of mast cells. Our findings may lead to the development of previously unreported antipruritic strategies.

RESULTS

Depressive effects of topical application of CCKs on SP-induced itch-associated response

We tested various CCKs for their ability to suppress scratching behavior induced by intradermal SP injection in ICR mice (Andoh *et al.*, 2001). We first examined the effect of percutaneously applied CCK on the response. Because CCK8S has an inhibitory ability in the CNS (Pommier *et al.*, 2002; Dufresne *et al.*, 2006) and gastrointestinal tract (Miyasaka *et al.*, 2004), CCK8S and the other CCK constructs consisting of smaller amino acids with or without sulfate (Table 1) were tested for their antipruritic activities. ICR mice were painted with various CCKs on the clipped, tape-stripped rostral part of the back skin (~1.8 cm^2) and then injected with SP intradermally at the CCK-painted site.

The topical application of CCK8S significantly reduced the scratching frequency, as compared with the nonapplied control (Figure 1a). Sulfated CCK7 (CCK7S) also reduced the scratching frequency, to a level comparable to that with CCK8S, whereas nonsulfated CCK8, CCK7, and CCK6 had no ability to suppress scratching. These results showed that CCKs have an antipruritic ability, and CCK constructs bearing sulfation of position 7 are required for the ability to suppress the scratching behavior. In this itch-associated-scratching model, we also administered CCK8S intradermally together with SP to mice. The scratching frequency induced by SP was profoundly suppressed by the simultaneous injection of CCK8S (Figure 1b). When the time course of effects induced by CCK8S was examined, both topical application (Figure 1c) and intradermal injection (Figure 1d) of CCKS reduced the scratching frequency at intervals of 0–5 minutes and 5–10 minutes.

These findings raised the possibility that epidermal and dermal cells participating in the development of itch are affected by CCKs.

Table 1. Amino acid sequences of CCK and its constructs

Sulfated CCK8 (CCK8S)	Asp–Tyr (SO_3–)–Met–Gly–Trp–Met–Asp–Phe–NH_2
Nonsulfated CCK8 (CCK8)	Asp–Tyr–Met–Gly–Trp–Met–Asp–Phe–NH_2
Sulfated CCK7 (CCK7S)	Tyr (SO_3–)–Met–Gly–Trp–Met–Asp–Phe–NH_2
Nonsulfated CCK7 (CCK7)	Tyr–Met–Gly–Trp–Met–Asp–Phe–NH_2
Nonsulfated CCK6 (CCK6)	Met–Gly–Trp–Met–Asp–Phe–NH_2

Abbreviation: CCK, cholecystokinin.

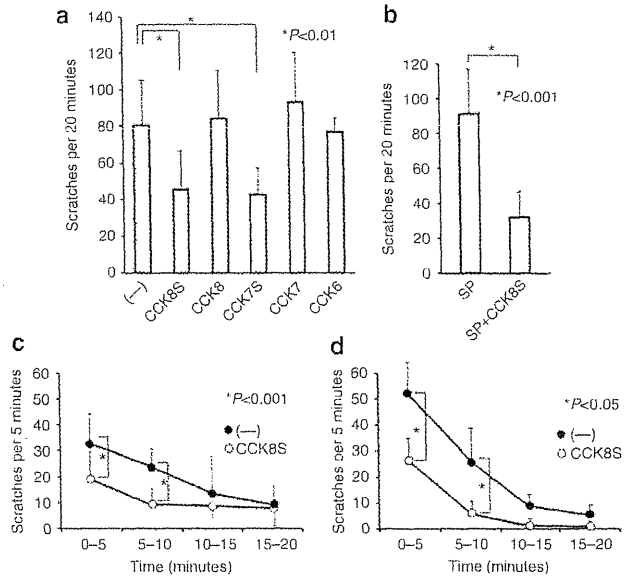

Figure 1. Suppression of substance P (SP)-induced itch by percutaneous application or intradermal injection of cholecystokinins (CCKs). (a) ICR mice were painted on the clipped skin with CCKs (0.5 nmol per site) and injected intradermally with SP (100 nmol per site). The group depicted with "(–)" represents mice injected with vehicle (acetone/olive oil) alone. The numbers of mice were as follows: CCK (—), $n=12$; CCK8S, $n=10$; CCK8, $n=6$; CCK7S, $n=6$; CCK7, $n=3$; and CCK6, $n=4$. (b) ICR mice were injected intradermally with SP or with SP and CCK8S. Each bar represents the mean of scratches per 20 minutes. CCK (–), $n=5$ and CCK8S, $n=8$. (c) Time course of scratching frequency in mice untreated ($n=12$) or topically administered CCK8S ($n=10$). (d) Time course of scratching frequency in mice untreated ($n=5$) or intradermally injected with CCK8S ($n=8$). CCK7, nonsulfated CCK7; CCK8, nonsulfated CCK8; CCK7S, sulfated CCK7; CCK8S, sulfated CCK8.

CCK2R expression in KCs and mast cells

Both KCs and mast cells are the possible targets of CCKs in the suppression of SP-induced pruritus. It is known that KCs express the receptors for itch-related molecules, neurokinin-1 receptor for SP, H1 receptor for histamine, and protease-activated receptor-2 for tryptase (synthetic agonist, SLIGRL-NH_2). Mast cells are well known to possess neurokinin-1 receptor (Scholzen *et al.*, 1998; Liu *et al.*, 2006). We investigated the expression of the CCK receptors CCK1R and CCK2R in KCs and mast cells. Primary cultures of KCs from ICR mice and fetal skin–derived mast cells (FSMCs) were collected, and mRNAs for CCK1R and CCK2R were quantitated by real-time PCR, RT-PCR, and western blotting analyses. The two types of cells expressed both CCK1R and CCK2R at the mRNA and protein levels (Figure 2). When the expression levels of real-time PCR analysis were normalized with the β-actin level, the two receptors were more highly expressed in FSMCs than in KCs.

In a preliminary DNA microarray analysis of normal human epidermal KCs, we investigated the levels of gene expression from stimulation with SP (10^{-6} M), histamine (10 μg ml^{-1}), or SLIGRL-NH_2 (100 nM) under high calcium (0.6 mM) concentration. The CCK2R expression by SP-stimulated KCs was most elevated; its level was $2^{8.67}$ times that of the control (Supplement Data online). Such an increased CCK2R expression was not observed with histamine or SLIGRL-NH_2. This observation suggested that CCK2R has an important role in the suppression of SP-stimulated KCs. To determine the effect of SP on KCs, ICR mouse KCs were incubated with SP for 30 minutes to 24 hours, and the expression of CCK2R and CCK1R was analyzed by western blotting. CCK2R was detected with antibodies as a 78 kDa band (Morisset *et al.*, 2003) and increased in KCs exposed to SP for 5 or 6 hours (Figure 3a). By contrast, CCK1R expression was not augmented by SP (Figure 3b). Thus, the expression of some receptors for CCK is enhanced by SP, depending on the receptor.

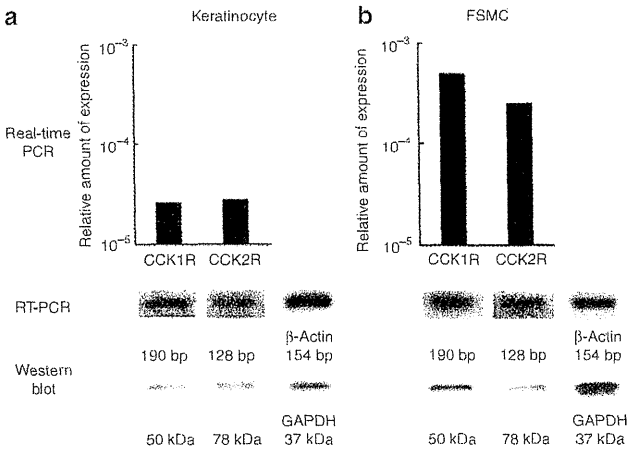

Figure 2. **CCK-A receptor (CCK1R) and CCK-B receptor (CCK2R) mRNA expression in keratinocytes and mast cells.** Cultured ICR mouse keratinocytes (**a**) and fetal skin–derived mast cells (FSMCs) (**b**) were examined for the expression of mRNAs for CCK1R and CCK2R using real-time PCR and RT-PCR and for the expression of their proteins using western blotting analysis. Data are expressed as the amount of expression relative to β-actin. Glyceraldehyde-3-phosphate dehydrogenase (GAPDH) was used as control for western blotting.

Suppression of FSMC degranulation by CCK8S with transient elevation of intracellular calcium

The above findings suggested that CCKs bind to CCK2R on KCs and mast cells and downmodulate their itch-related biological functions. Given that the level of CCK2R expression was higher in FSMCs than in KCs and the application of CCKs immediately exerted its inhibitory effects on the scratching behavior, it is possible that CCKs directly affect mast cells. We therefore focused on mast cells as the primary target. The addition of compound 48/80 induced degranulation of FSMCs (Figure 4a). This promoted degranulation of FSMCs, which was significantly inhibited by CCK8S at 10^{-8} or 10^{-7} M concentration.

To test whether CCK8S evokes signal transduction in mast cells, we measured the intracellular calcium using confocal recording. The fluorescence intensity of 15 cells positively responding on addition of CCK8S was monitored with computerized color change on a display using a digital image processing system. The mast cells exhibiting green fluorescence of Fluo-4-AM at any time point between 40 and

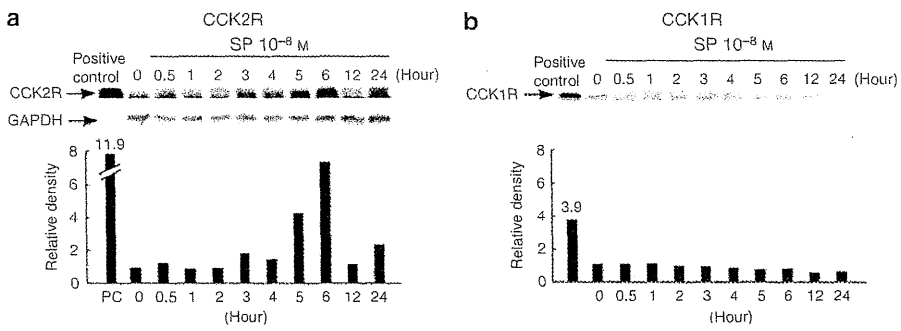

Figure 3. **Western blotting of CCK-A receptor (CCK1R) and CCK-B receptor (CCK2R) in mouse keratinocytes stimulated with substance P (SP).** ICR mouse keratinocytes were incubated with SP (10^{-8} M) for 0.5–24 hours and harvested at each time point. The expression levels of CCK2R (**a**) and CCK1R (**b**) were analyzed by western blotting. NIH/3T3 whole lysates were used as positive control. Glyceraldehyde-3-phosphate dehydrogenase (GAPDH) was used as control for western blotting and exhibited similar intensities in the samples cultured for 0–24 hours. The intensity of each band was subjected to densitometric analysis and expressed as density relative to the nontreated control (0).

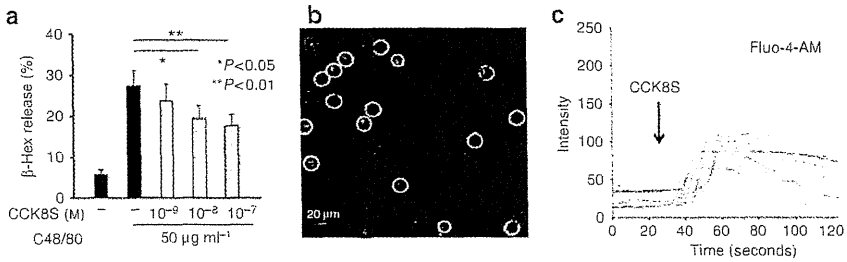

Figure 4. Suppression of fetal skin-derived mast cell (FSMC) degranulation by sulfated CCK8 (CCK8S) with transient intracellular calcium increase. (**a**) FSMCs were incubated with or without CCK8S in the presence of compound 48/80 (C48/80; 50 μg ml^{-1}) for 15 minutes. Supernatants and cell lysates were incubated with *p*-nitrophenyl-*N*-acetyl-β-D-galactosaminide, and β-hexosaminidase (β-Hex) release was determined as the ratio between activity in the supernatant and cell lysate, multiplied by 100. (**b**) FSMCs were loaded with Fluo-4-AM (green) and stained for CD117 (c-kit, red). The percentage of CCK8S-responding FSMCs was determined from the fluorescence traces of all cells. Circles represent responding FSMCs and squares represent nonresponding FSMCs. Bar = 20 μm. (**c**) The addition of CCK8S to FSMC culture induced an increase in intracellular calcium level.

80 seconds after CCK8S addition were defined as positively responding cells (Figure 4b and c); these are marked with a yellow circle in Figure 4b. The addition of CCK8S to the FSMC culture induced a prompt rise of calcium that persisted for more than 2 minutes and then gradually declined, indicating that CCK8S induces signaling via CCK2R in mast cells. The percentage of responding FSMCs was determined from the fluorescence traces of all cells. As shown in Figure 4b, in which circles and squares represent CCK8S-responding and nonresponding FSMCs, respectively, 45% (16 of 36 cells) of FSMCs were typically activated by CCK8S.

DISCUSSION

Despite their original name of cholecyst stimulators, CCKs have been known to serve as CNS modulators (Dufresne *et al.*, 2006) and CCK8S downmodulates opioid responses (Pommier *et al.*, 2002; Agnes *et al.*, 2008). As suggested in our present study, CCKs may also have a function of downmodulator in the peripheral itch. The topical application of CCKs suppressed the itch-related scratching behavior evoked by SP injection. The expression of CCK2R, but not CCK1R, in murine and human KCs was markedly enhanced by exposure to SP. It is likely that CCK2R, whose expression is augmented by SP, has a down-regulatory role in the excess peripheral itch.

Among the CCK constructs consisting of different numbers of amino acids with or without sulfate, CCK8S and CCK7S, but not CCK8, CCK7, or CCK6, exerted an antipruritic action. Therefore, in a comparison between CCK8S and CCK8 and between CCK7S and CCK7, sulfation of position 7 is required for the ability to suppress the scratching behavior. This is in accordance with the observation that CCK8S has an anxiogenic effect (Harro, 2006), a depressant effect, and an anti-opioid effect (Noble *et al.*, 1999), but the effects of CCK are limited by desulfation of the tyrosine (Tokunaga *et al.*, 1993).

Although the exact mode of antipruritic action of CCKs is still speculative, some informative observations were obtained from the study. Both percutaneous application and dermal injection were effective routes for CCK8S in suppressing itch, suggesting that epidermal and/or dermal constituents are the targets of CCKs. Furthermore, the administration of CCK8S rapidly inhibited the SP-induced itch. We thus investigated the mechanism of CCK suppression of itch in *in vitro* studies, focusing on mast cells. CCK8S significantly reduced the degranulation of FSMCs with elevation of intracellular calcium concentration, suggesting that mast cell degranulation is inhibited by CCK8S through CCK2R. Alternatively, or additionally, KCs are possibly involved in CCR action. KCs are thought to mediate pruritus by releasing inflammatory mediators and neurotrophins. Therefore, the antipruritic effect of CCK8S on KCs, if any, seems to need a time lag to operate. As the therapeutic action of topical CCK8S is rapid, mast cells may be more likely targeted by CCK8S than KCs. The high expression of CCK2R in mast cells further supports the notion that mast cells are sensitive to CCKs. However, SP was reported to cause scratching behavior in both mast cell-deficient and wild-type mice (Hossen *et al.*, 2003), suggesting a mast cell-independent mechanism of SP-evoked itch. Given this observation, it is possible that another skin constituent, such as the sensory nerves, is affected by CCKs. The target cells and the actions of CCK8S on them warrant elucidation in the future.

The antipruritic effects of CCK8S and CCK7S on this mouse itch model may afford a therapeutic use for the CCKs for the treatment of skin diseases with peripheral itch. Given that the major target of CCKs is mast cells, urticaria, atopic dermatitis, contact dermatitis, and other types of eczematous dermatitis would be successfully treated with CCKs topically applied to the skin. The therapeutic effects of CCKs on peripheral itch may shed light on the mechanisms underlying the physiological regulation of itch, and it is notable that CCKs have potential as a topical drug for pruritic skin diseases.

MATERIALS AND METHODS

Animals

Female ICR mice were obtained from KBT Oriental (Tosu, Japan). These mice were maintained in the Laboratory Animal Research Center of the University of Occupational and Environmental Health under specific-pathogen-free conditions and used at the age of 6–8 weeks. All animal experiments were performed according to the guidelines approved by our university for the care and use of animals.

Reagents

SP, CCK8S, nonsulfated CCK8, CCK7S, and nonsulfated CCK6 were purchased from the Peptide Institute (Osaka, Japan). Nonsulfated

CCK7 was purchased from Funakoshi (Tokyo, Japan). Compound 48/80 was purchased from Sigma (St Louis, MO).

Itch-associated scratching behavior and topical application of CCKs

The hair was clipped over the rostral part of the each mouse's back 1 or 2 days before the experiment. Before behavioral recording, each animal (four per observation) was put into an acrylic cage (18 × 23 × 11 cm) for at least 1 hour for acclimation. An intradermal injection of SP (100 nmol in 50 µl of physiological saline per site) induced scratching of the skin around the injected site with the hindpaws (Andoh *et al.*, 2001). CCKs were topically applied in two ways: percutaneous application and intradermal injection. For percutaneous application, the shaved back skin was stripped with Scotch tape (3 M) six times on the day before the experiment (Nishijima *et al.*, 1997). The clipped backs of the mice were painted (1.8 cm^2, 1.5 cm in diameter) with 20 µl CCK (0.5 nmol per site) in acetone/olive oil (3:1) 3–4 minutes before the SP injection (100 nmol per site). For intradermal application, mice were injected intradermally with CCK (0.5 nmol per site in 20 µl physiological saline), followed immediately by SP injection at the same site (100 nmol per site). Immediately after treatment, the animals were put back into the same cage and their behavior was videotaped for 40 minutes using a digital video camera (Andoh *et al.*, 2001). Using the video, the frequency of scratching toward the injected site by the hindpaws was recorded for the first 20 minutes.

Murine KCs

The skin of ICR newborn mice was peeled within 24 hours after birth and incubated with 0.05% collagenase (collagenase from *Clostridium histolyticum* type 2; Sigma) for 2 days at 37 °C in a 5% CO_2 atmosphere. Epidermal sheets were collected and suspended in culture medium. Cell suspension was plated into six-well plates (Corning Glass Works, Corning, NJ) and grown to subconfluence in CnT-07 medium (Funakoshi).

Murine mast cells

The method for preparation of murine FSMCs has been described previously (Yamada *et al.*, 2003). Day 14 fetal skin was dissociated by 0.25% trypsin for 20 minutes at 37 °C in Hank's balanced salt solution (Gibco, Carlsbad, CA). Erythrocytes were lysed using RBC-lysing buffer (Sigma) and, after washing, cells were resuspended in complete RPMI, which is RPMI-1640 (Gibco) supplemented with 5% fetal bovine serum (Gibco), 1% nonessential amino acids (Gibco), 1% sodium pyruvate (Gibco), antibiotic/antimycotic (Invitrogen, Carlsbad, CA), and 0.1% 2-mercaptoethanol (Gibco). Fifty milliliters of the cell suspension in each 175 cm^2 75-flask (Corning Glass Works) was cultured in the presence of 20 ng ml^{-1} recombinant mouse IL-3 (Invitrogen) and 20 ng ml^{-1} recombinant mouse stem cell factor (Biosource, Camarillo, CA) at 37 °C without changing the medium. Nonadherent and loosely adherent cells were harvested. The cells were centrifuged and resuspended in RPMI, layered on 40% Percoll (GE Healthcare, Buckinghamshire, England), and centrifuged at room temperature. The cell pellet at the bottom was used as FSMCs. For flowcytometric analysis, cells were stained with phycoerythrin-conjugated anti-mouse FcεRI (eBioscience, San Diego, CA) and Alexa Fluor 700-conjugated anti-mouse CD117 (c-kit; eBioscience) for 20 minutes on ice, washed twice, and then resuspended with FACS buffer. Flow cytometric analysis was performed with FACS Canto (BD, Franklin Lakes, NJ) and FlowJo software (TreeStar, San Carlos, CA). The purity of FSMCs was 95%, as determined by both FcεRI and CD117 positivity by flow cytometry.

Real-time quantitative RT-PCR analysis

Total RNA was extracted from the cell pellet using the PureLink RNA Mini Kit (Invitrogen). cDNA was reverse transcribed from total RNA samples using the TaqMan Reverse Transcription reagents (Applied Biosystems, Carlsbad, CA). mRNA expression was quantified by real-time PCR using SYBR Green Dye (PE Biosystems, Foster City, CA) with an ABI PRISM 7000 Sequence Detection System (Applied Biosystems) according to the manufacturer's instructions. Primers were designed using Primer Bank for the human and murine genes, and they were constructed by Invitrogen. The sequences are as follows: murine β-actin: 5′-GGCTGTATTCCCCTCCATCG-3′ and 5′-CCAGTTGGTAACAATGCCATGT-3′; murine CCK2R: 5′-GATGG CTGCTACGTGCAACT-3′ and 5′-CGCACCACCCGCTTCTTAG-3′; and murine CCK1R: 5′-CACGCTGGTTATCACGGTG-3′ and 5′-GC CCATGAAGTAGGTGGTAGTC-3′. The conditions for the real-time PCR were as follows: 2.0 minutes at 50 °C, 10 minutes at 95 °C, and then 50 cycles of amplification consisting of 15 seconds at 95 °C and 1 minute at 60 °C. All heating and cooling steps were performed with a slope of 20 °C per second. Relative expression was calculated using the delta Ct method.

Western blotting

KCs from ICR mice were stimulated with SP (10^{-8} M) in six-well plates (Corning Glass Works) for 0.5–24 hours, harvested with a rubber policeman, and subjected to extraction with RIPA buffer (Wako, Osaka, Japan; 50 mM Tris-HCl (pH8.0), 150 mM sodium chloride, 0.5% (wt/vol) sodium deoxycholate, 0.1% (wt/vol) SDS, and 1.0% (wt/vol) NP-40 substitute). Protein samples (20 ìg) were separated by 8% SDS-polyacrylamide gel electrophoresis and electroblotted onto polyvinylidene difluoride membranes for 2 hours at 180 mA. After blocking with 5% skim milk solution, the membranes were incubated with rabbit anti-mouse CCK1R (SC-33220; 1:1,000, Santa Cruz, Santa Cruz, CA), CCK2R (SC-33221; 1:1,000, Santa Cruz) polyclonal antibodies, or GAPDH (SC-25887; 1:1,000, Santa Cruz), and the reaction was detected with horseradish peroxidase–conjugated goat anti-rabbit IgG (1:3,000, Bio-Rad, Hercules, CA). Immunoblots were visualized using the ECL Plus Western Blotting Detection Reagents (GE Healthcare) according to the manufacturer's protocol. Bands were quantified by densitometry with the help of a CS Analyzer version 2.0 (ATTO, Tokyo, Japan). NIH/3T3 whole cell lysate (Santa Cruz) was used as a positive control.

Mast cell degranulation

Degranulation of FSMCs was assessed by β-hexosaminidase assay (Yamada *et al.*, 2003; Noguchi *et al.*, 2005). FSMCs were washed with Tyrode's buffer (Sigma) and resuspended at a concentration of 2×10^4 cells per well into a 96-well plate. FSMCs were incubated with or without CCK8S in the presence of compound 48/80 (50 µg ml^{-1}) for 15 minutes at 37 °C. The plate was centrifuged for 5 minutes, and the supernatants were placed into another 96-well plate. Cell pellets were resuspended in Tyrode's buffer containing 0.5% triton X-100 (Sigma). Supernatants and cell lysates (50 µl) were incubated with 100 µl of 2.5 mM *p*-nitrophenyl-*N*-acetyl-β-D-galactosaminide (Sigma),

dissolved in 0.04 mM citrate buffer (pH 4.5), at 37 °C for 90 minutes. The reaction was stopped with 100 µl of 0.4 M glycine (pH 10.7; MP Biomedicals, Solon, OH). The plate was read at 405 nm using a 595 nm reference filter in a microplate reader (Bio-Rad). β-Hexosaminidase release was determined as the ratio between activity in the supernatant and the cell lysate, multiplied by 100.

Calcium influx determined by confocal imaging

Confocal imaging of cells loaded with fluorescent dyes was performed using a Zeiss LSM5 pascal (Carl Zeiss, Jena, Germany). FSMCs were loaded with Fluo-4-AM (Invitrogen; 1 µM) at 37 °C for 20 minutes, washed twice, and set aside for at least 40 minutes. FSMCs were also stained for CD117 (c-kit) with Alexa Fluor 700–conjugated anti-mouse CD117 antibody. The LSM5 multitrack configuration was used for simultaneous measurement of intracellular calcium concentration (excitation, 488 nm; emission, long-pass 505 nm filter) and the expression of CD117 (excitation, 633 nm; emission, long-pass 650 nm filter). Images were recorded (usually recording for 300 seconds) at room temperature, in a 512 × 512-pixel format. As stimulants, SP or CCKs were added directly to the bath as a small drop (10 µl; final concentration, 10^{-6} M SP and 10^{-6} M CCK8S). Image data were analyzed offline using the Zeiss LSM510 analyzing software (LSM Image Examiner, Carl Zeiss). The mast cells exhibiting green fluorescence of Fluo-4-AM at any time point between 40 and 80 seconds after CCK8S addition were defined as positively responding cells.

Gene-array analysis

Normal human epidermal KCs were cultured with SP (10^{-6} M), histamine (10 mg ml^{-1}), and SLIGRL-NH_2 (100 nM) for 2 hours and harvested. For DNA microarray analysis, total RNA was extracted from Normal human epidermal KCs with the RNeasy Mini Kit (Qiagen, Valencia, CA). Images were analyzed with the DNASIS Array (DNA Chip Research, Hitachi Software Engineering, Tokyo, Japan) according to the manufacturer's instructions. The results of DNA microarray analysis of the top and bottom 20 genes with respect to expression levels induced by SP, histamine, or SLIGRL-NH_2 are shown in the Supplementary Data online.

Statistical analysis

Data were analyzed using an unpaired Student's *t*-test. $P<0.05$ was considered to be significant.

CONFLICT OF INTEREST

The authors state no conflict of interest.

ACKNOWLEDGMENTS

This study was supported by a grant from the Ministry of Education, Science, Sports and Culture and a grant from the Ministry of Health, Labour and Welfare, Japan. We thank Yukako Miyazaki and Rie Murase for their technical assistance.

SUPPLEMENTARY MATERIAL

Supplementary material is linked to the online version of the paper at http://www.nature.com/jid

REFERENCES

Agnes RS, Ying J, Kover KE *et al.* (2008) Structure-activity relationships of bifunctional cyclic disulfide peptides based on overlapping pharmacophores at opioid and cholecystokinin receptors. *Peptides* 29:1413–23

Andoh T, Katsube N, Maruyama M *et al.* (2001) Involvement of leukotriene B(4) in substance P-induced itch-associated response in mice. *J Invest Dermatol* 117:1621–6

Bonetto V, Jornvall H, Andersson M *et al.* (1999) Isolation and characterization of sulphated and nonsulphated forms of cholecystokinin-58 and their action on gallbladder contraction. *Eur J Biochem* 264:336–40

Dufresne M, Seva C, Fourmy D (2006) Cholecystokinin and gastrin receptors. *Physiol Rev* 86:805–47

Harro J (2006) CCK and NPY as anti-anxiety treatment targets: promises, pitfalls, and strategies. *Amino Acids* 31:215–30

Hossen MA, Sugimoto Y, Kayasuga R *et al.* (2003) Involvement of histamine H3 receptors in scratching behaviour in mast cell-deficient mice. *Br J Dermatol* 149:17–22

Ikoma A, Steinhoff M, Ständer S *et al.* (2006) The neurobiology of itch. *Nat Rev Neurosci* 7:535–47

Liu JY, Hu JH, Zhu QG *et al.* (2006) Substance P receptor expression in human skin keratinocytes and fibroblasts. *Br J Dermatol* 155:657–62

Ma KT, Si JQ, Zhang ZQ *et al.* (2006) Modulatory effect of CCK-8S on GABA-induced depolarization from rat dorsal root ganglion. *Brain Res* 1121:66–75

Miyasaka K, Ohta M, Kana S *et al.* (2004) Enhanced gastric emptying of a liquid gastric load in mice lacking cholecystokinin-B receptor: a study of CCK-A,B,and AB receptor gene knockout mice. *J Gastroenterol* 39:319–23

Mollereau C, Roumy M, Zajac JM (2005) Opioid-modulating peptides: mechanisms of action. *Curr Top Med Chem* 5:341–55

Moriarty P, Dimaline R, Thompson DG *et al.* (1997) Characterization of cholecystokininA and cholecystokininB receptors expressed by vagal afferent neurons. *Neuroscience* 79:905–13

Morisset J, Julien S, Lainé J (2003) Localization of cholecystokinin receptor subtypes in the endocine pancreas. *J Histochem Cytochem* 51:1501–13

Nishijima T, Tokura Y, Imokawa G *et al.* (1997) Altered permeability and disordered cutaneous immunoregulatory function in mice with acute barrier disruption. *J Invest Dermatol* 109:175–82

Noble F, Wank SA, Crawley JN *et al.* (1999) International union of Pharmacology. XXI. Structure, distribution, and functions of cholecystokinin receptors. *Pharmacol Rev* 51:745–81

Noguchi J, Kuroda E, Yamashita U (2005) Strain difference of murine bone marrow-derived mast cell functions. *J Leukoc Biol* 78:605–11

Ohkubo H, Nakanishi S (1991) Molecular characterization of the three tachykinin receptors. *Ann NY Acad Sci* 632:53–62

Pommier B, Beslot F, Simon A *et al.* (2002) Deletion of CCK2 receptor in mice results in an upregulation of the endogenous opioid system. *J Neurosci* 22:2005–11

Rehfeld JF, Friis-Hansen L, Goetze JP *et al.* (2007) The biology of cholecystokinin and gastrin peptides. *Curr Top Med Chem* 7:1154–65

Scholzen T, Armstrong CA, Bunnett NW *et al.* (1998) Neuropeptides in the skin: interactions between the neuroendocrine and the skin immune systems. *Exp Dermatol* 7:81–96

Steinhoff M, Bienenstock J, Schmelz M *et al.* (2006) Neurophysiological, neurological, and neuroendocrine basis of pruritus. *J Invest Dermatol* 126:1705–18

Tokunaga Y, Cox KL, Coleman R *et al.* (1993) Characterization of cholecystokinin receptors on the human gall bladder. *Surgery* 113:155–62

Wiesenfeld-Hallin Z, de Araújo Lucas G, Alster P *et al.* (1999) Cholecystokinin/opioid interactions. *Brain Res* 848:78–89

Yamada N, Matsushima H, Tagaya Y *et al.* (2003) Generation of a large number of connective tissue type mast cells by culture of murine fetal skin cells. *J Invest Dermatol* 121:1425–32

Yamaguchi J, Nakamura F, Aihara M *et al.* (2008) Semaphorin3A alleviates skin lesions and scratching behavior in NC/Nga mice, an atopic dermatitis model. *J Invest Dermatol* 128:2842–9

Yosipovitch G, Papoiu AD (2008) What causes itch in atopic dermatitis? *Curr Allergy Asthma Rep* 8:306–11

Zheng Y, Akgun E, Harikumar KG *et al.* (2009) Induced association of mu opioid (MOP) and type 2 cholecystokinin (CCK2) receptors by novel bivalent ligands. *J Med Chem* 52:247–58